Available online at www.sciencedirect.com
ScienceDirect
Journal of Sound and Vibration 298 (2006) 154–179
JOURNAL OF SOUND AND VIBRATION
www.elsevier.com/locate/jsvi

Double Neimark–Sacker bifurcation and torus bifurcation of a class of vibratory systems with symmetrical rigid stops

G.W. Luo[a,*], Y.D. Chu[a], Y.L. Zhang[b], J.G. Zhang[a]

[a]*School of Mathematics, Physics and Software Engineering, Lanzhou Jiaotong University, Lanzhou 730070, PR China*
[b]*School of Mechatronic Engineering, Lanzhou Jiaotong University, Lanzhou 730070, PR China*

Received 14 July 2004; received in revised form 18 August 2005; accepted 24 April 2006
Available online 17 August 2006

Abstract

A multidegree-of-freedom system having symmetrically placed rigid stops and subjected to periodic excitation is considered. The system consists of linear components, but the maximum displacement of one of the masses is limited to a threshold value by the symmetrical rigid stops. Repeated impacts usually occur in the vibratory system due to the rigid amplitude constraints. Such models play an important role in the studies of mechanical systems with clearances or gaps. Double Neimark–Sacker bifurcation of the system is analyzed by using the center manifold and normal form method of maps. The period-one double-impact symmetrical motion and homologous disturbed map of the system are derived analytically. A center manifold theorem technique is applied to reduce the Poincaré map to a four-dimensional one, and the normal form map associated with double Neimark–Sacker bifurcation is obtained. The bifurcation sets for the normal-form map are illustrated in detail. Local behavior of the vibratory systems with symmetrical rigid stops, near the points of double Neimark–Sacker bifurcations, is reported by the presentation of results for a three-degree-of-freedom vibratory system with symmetrical stops. The existence and stability of period-one double-impact symmetrical motion are analyzed explicitly. Also, local bifurcations at the points of change in stability are analyzed, thus giving some information on dynamical behavior near the points of double Neimark–Sacker bifurcations. Near the value of double Neimark–Sacker bifurcation there exist period-one double-impact symmetrical motion and quasi-periodic impact motions. The quasi-periodic impact motions are represented by the closed circle and "tire-like" attractor in projected Poincaré sections. With change of system parameters, the quasi-periodic impact motions usually lead to chaos via "tire-like" torus doubling.

1. Introduction

Vibrating systems with clearances, gaps or stops are frequently encountered in technical applications of mechanism, vehicle traffic and nuclear reactor, etc. Repeated impacts, i.e., vibro-impacts, usually occur whenever the components of a vibrating system collide with rigid obstacles or with each other. The principle of operation of vibration hammers, impact dampers, inertial shakers, pile drivers, offshore structures, machinery for compacting, milling and forming, etc., is based on the impact action for moving bodies. With other equipment, e.g., mechanisms with clearances, heat exchangers, fuel elements of nuclear reactors, gears, piping

*Corresponding author.
E-mail addresses: luogw@mail.lzjtu.com, luogw@hotmail.com (G.W. Luo).

0022-460X/$ - see front matter © 2006 Elsevier Ltd. All rights reserved.
doi:10.1016/j.jsv.2006.04.025

systems, wheel–rail interaction of high-speed railway coaches, etc., impacts also occur, but they are undesirable as they bring about failures, strain, shorter service life and increased noise levels. Researches into vibro-impact dynamics have important significance on optimization design of machinery with clearances or stops, noise suppression and reliability analysis, etc. The physical process during impacts is of strongly nonlinear and discontinuous characteristics. Therefore, application of standard analytical tools based on linearization will fail to capture essential ingredients of the response. The presence of the nonlinearity and discontinuity complicates the dynamic analysis of repeated impact systems considerably, but it can be described theoretically and numerically by discontinuities in good agreement with reality. Compared with single impact, the vibro-impact dynamics is more complicated, and hence, has received great attention. Many new problems of theory have been advanced in researches into vibro-impact dynamics, and the study of vibro-impact problems becomes a new subject on nonlinear dynamics. Some important problems on vibro-impact dynamics, including global bifurcations [1–10], singularities [11–19], chattering impact [20], quasi-periodic impacts [21–24] and controlling chaos [25], etc., have been studied in the past several years. Along with the basic researches into vibro-impact dynamics, the researches into application to these systems are developed, for example, wheel–rail impact of railway coaches [26–28], impact noise analysis [29,30], inertial shakers [31,32], vibrating hammer [33], offshore structure [34], impact dampers [35–40] and gears [41–44], etc.

A multidegree-of-freedom system having symmetrically placed rigid stops and subjected to periodic excitation is considered. The system consists of linear components, but the maximum displacement of one of the masses is limited to a threshold value by the symmetrical rigid stops. Such models play an important role in the basic research of vibro-impact dynamics. As a result, the majority of the previous work idealizes analyses of stability, bifurcation and singularity of these systems as single-degree-of-freedom oscillators with rigid stops by analytical and numerical approaches, e.g., see Refs. [1–6,11–17,33]. Periodic-impact motions and bifurcations of two-degree-of-freedom systems with rigid stops are analyzed by numerical simulation in Refs. [7,8,22–24,26,27]. Finally, Bernardo [19] study C-bifurcations of multidegree-of-freedom systems with rigid stops and give the normal form map of C-bifurcations. The other references, in the paper, consider the vibratory systems with soft stops (see Refs. [21,25,28,34]) and the systems of which components collide with each other(see Refs. [31,32,35–42]). The present analysis extends the previous work on vibratory system with rigid stops by developing an efficient way of determining exact periodic motions and local bifurcations for a general multiple-degree-of-freedom system, with a component that possesses symmetrically placed rigid stops. The purpose of the study is to focus attention on stability and codimensiom two bifurcations of period-one double-impact symmetrical motion of the system. There are many types of codimension two bifurcations of ordinary differential equations and maps, some of which have been studied in Refs. [45–49]. Double Neimark–Sacker bifurcation of the vibratory systems with symmetrical rigid stops is investigated in the paper. The existence, stability and local bifurcations of period-one double-impact symmetrical motion are analyzed explicitly. Local behavior of the vibratory systems with symmetrical rigid stops, near the points of double Neimark–Sacker bifurcations, is reported by the presentation of results for a three-degree-of-freedom vibratory system with symmetrical rigid stops.

2. Mechanical model

A multidegree-of-freedom system having symmetrically placed rigid stops and subjected to periodic excitation is shown in Fig. 1. Displacements of the masses $M_1, M_2, \ldots, M_{n-1}$ and M_n are represented by $X_1, X_2, \ldots, X_{n-1}$, and X_n, respectively. The masses are connected to linear springs with stiffnesses $K_1, K_2, \ldots, K_{n-1}$ and K_n, and linear viscous dashpots with damping constants, $C_1, C_2, \ldots, C_{n-1}$ and C_n. Damping in the mechanical model is assumed as proportional damping of the Rayleigh type. The excitations on the masses are harmonic with amplitudes $P_1, P_2, \ldots, P_{n-1}$ and P_n. The excitation frequency Ω and phase angle τ are the same for these masses. The masses move only in the horizontal direction. For small forcing amplitudes the system will undergo simple oscillations and behave as a linear system. As the amplitude is increased, the kth mass M_k eventually begins to hit the stops and the motion becomes nonlinear (the other masses are not allowed to impact any rigid stop). The impact is described by a coefficient of restitution R, and it is assumed that the duration of impact is negligible compared to the period of the force.

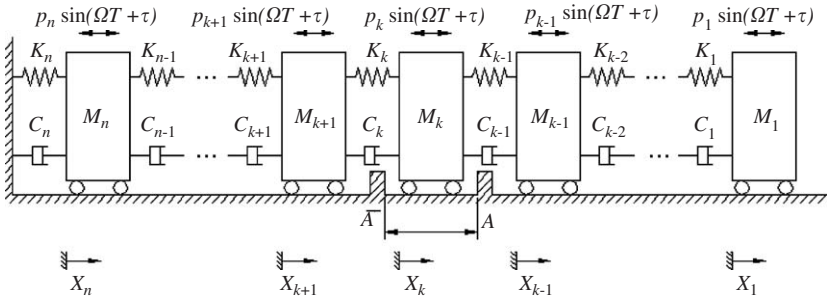

Fig. 1. Schematic of a multi-degree-of-freedom vibratory system with symmetrical rigid stops.

Suppose $M_1 \neq 0$, $K_1 \neq 0$, and let $F_0 = |P_1| + |P_2| + \cdots + |P_k| + \cdots + |P_n|$. The non-dimensional quantities are given by

$$m_i = \frac{M_i}{M_1}, \quad k_i = \frac{K_i}{K_1}, \quad f_{i0} = \frac{P_i}{F_0}, \quad \zeta_i = \frac{C_i}{2\sqrt{K_1 M_1}}, \quad x_i = \frac{X_i K_1}{F_0}, \quad \gamma = \zeta_i / k_i,$$
$$\omega = \Omega\sqrt{\frac{M_1}{K_1}}, \quad t = T\sqrt{\frac{K_1}{M_1}}, \quad \delta = \frac{BK_1}{F_0}, \quad i = 1, 2, \ldots, k, \ldots, n. \tag{1}$$

The motion processes of the system, between consecutive impacts occurring at the stop A, are considered. Between any two consecutive impacts, the time T is always set to zero directly at the starting point A (the mass M_k departing from the $X_k = B$ stop with negative velocity), and the phase angle τ is used only to make a suitable choice for the origin of time in the calculation. The state of the vibro-impact system, immediately after impact, has become new initial conditions in the subsequent process of the motion. Between the stops, the non-dimensional differential equations of motion are given by

$$M\ddot{x} + C\dot{x} + Kx = F\sin(\omega t + \tau) \quad (|x_k| < \delta), \tag{2}$$

where a dot $(\cdot)$ denotes differentiation with to the non-dimensional time t, and M, C, K are the non-dimensional mass, damping and stiffness matrixes, respectively, $x = (x_1, x_2, \ldots, x_n)^{\mathrm{T}}$, $F = (f_{10}, f_{20}, \ldots, f_{n0})^{\mathrm{T}}$.

When the impacts occur, for $|x_k| = \delta$, the velocities of the impacting mass M_k are changed according to the impact law

$$\dot{x}_{kA+} = -R\dot{x}_{kA-}, \quad (x_k = \delta), \quad \dot{x}_{k\bar{A}+} = -R\dot{x}_{k\bar{A}-}, \quad (x_k = -\delta), \tag{3}$$

where $\dot{x}_{kA-}$ and $\dot{x}_{kA+}$ ($\dot{x}_{k\bar{A}-}$ and $\dot{x}_{k\bar{A}+}$) represent the impacting mass' velocities of approach and departure at the instant of impacting with the stop $A(\bar{A})$, respectively.

3. Period-one double-impact symmetrical motion and disturbed map

Impacting systems are conveniently studied by use of a mapping derived from the equations of motion. Each iterate of this map corresponds to the mass M_k striking the stop A once we can characterize periodic motions of the vibratory system with symmetrical rigid stops by the symbol n–p–q, where q and p is the number of impacts occurring, respectively, at the constraint A and $\bar{A}$, and n is the number of the forcing cycles. In this section, only the periodic motion of the model, with two symmetrical impacts per force cycle, is considered, which is called the period-one double-impact symmetrical motion. Let us choose the Poincaré section $\sigma = \{(x_1, \dot{x}_1, x_2, \dot{x}_2, \ldots, x_k, \dot{x}_k, \ldots, x_n, \dot{x}_n, \theta) \in \boldsymbol{R}^{2n} \times \boldsymbol{S}, x_k = \delta, \dot{x}_k = \dot{x}_{k+}\}$ to establish the Poincaré map of the vibratory system with symmetrical rigid stops. The period-one double-impact symmetrical motion and its disturbed map have been derived analytically in Appendix A. Here, the disturbed map of period-one double-impact symmetrical motion is represented briefly by

$$X' = \tilde{f}(v, X), \tag{4}$$

where $\theta = \omega t$, $X \in \boldsymbol{R}^{2n}$, v is real parameter, $v \in \boldsymbol{R}^1$ or $\boldsymbol{R}^2$; $X = X^* + \Delta X$, $X' = X^* + \Delta X'$; $X^* = (x_{10}, x_{20}, \ldots, x_{(k-1)0}, \tau_0, x_{(k+1)0}, \ldots, x_{n0}, \dot{x}_{10}, \dot{x}_{20}, \ldots, \dot{x}_{(k-1)0}, \dot{x}_{k+}, \dot{x}_{(k+1)0}, \ldots, \dot{x}_{n0})^{\mathrm{T}}$ is a fixed point in the hyper-

plane σ, the disturbed vectors of X^* are represented by

$$\Delta X = (\Delta x_1, \Delta x_2, \ldots, \Delta x_{k-1}, \Delta\tau, \Delta x_{k+1}, \ldots, \Delta x_n, \Delta\dot{x}_1, \Delta\dot{x}_2, \ldots, \Delta\dot{x}_{k-1}, \Delta\dot{x}_{k+}, \Delta\dot{x}_{k+1}, \ldots, \Delta\dot{x}_n)^{\mathrm{T}},$$

$$\Delta X' = (\Delta x'_1, \Delta x'_2, \ldots, \Delta x'_{k-1}, \Delta\tau', \Delta x'_{k+1}, \ldots, \Delta x'_n, \Delta\dot{x}'_1, \Delta\dot{x}'_2, \ldots, \Delta\dot{x}'_{k-1}, \Delta\dot{x}'_{k+}, \Delta\dot{x}'_{k+1}, \ldots, \Delta\dot{x}'_n)^{\mathrm{T}}.$$

Map (5) can be changed by

$$\Delta X' = \tilde{f}(v, X) - X^* \stackrel{\mathrm{Def}}{=} f(v, \Delta X). \tag{5}$$

Linearizing the Poincaré map at the fixed point X^* results in the matrix

$$Df(v,0) = \left.\frac{\partial f(v,\Delta X)}{\partial \Delta X}\right|_{(v,\underbrace{0,0,\ldots,0}_{2n})}. \tag{6}$$

The stability of 1-1-1 symmetrical motion is determined by computing and analyzing eigenvalues of $Df(v,0)$. Variations of the parameters of the system will cause the fixed point and its associated eigenvalues to move. If one of them passes through the unit circle in the complex plane, i.e.,$\left|\lambda_i(v_c) = 1\right|$ (v_c is a bifurcation value), an instability and an associated bifurcation will occur. In general, bifurcation occurs in various ways according to the numbers of the eigenvalues on the unit circle and their position on the unit circle. Here, we shall consider the case of $v \in \boldsymbol{R}^2$, and dynamics of the system is studied with special attention to double Neimark–Sacker bifurcation associated with 1-1-1 symmetrical motion.

4. Center manifold and normal form map

Let us consider the map $X' = \tilde{f}(v, X)$, in which $v \in \boldsymbol{R}^2$. X^* is a fixed point for the map for v in some neighborhood of a critical value $v = v_c$ at which $Df(v,0)$ satisfies the following assumptions:

H.1. Jacobian matrix $Df(v,0)$ has two complex conjugate pairs of eigenvalues $\lambda_{1,2}(v_c)$ and $\lambda_{3,4}(v_c)$ on the unit circle, i.e., $\lambda_2(v_c) = \bar{\lambda}_1(v_c)$ and $\left|\lambda_{1,2}(v_c)\right| = 1$; $\lambda_4(v_c) = \bar{\lambda}_3(v_c)$and $\left|\lambda_{3,4}(v_c)\right| = 1$.

H.2. the remainder of the spectrum of $Df(v,0)$ are strictly inside the unit circle.

For all v in some neighborhood of v_c, the map $\Delta X' = f(v, \Delta X)$, under the change of variables $\mu_1 = v_1 - v_{1c}$, $\mu_2 = v_2 - v_{2c}$, $\mu = (\mu_1, \mu_2)^{\mathrm{T}}$ and $\Delta X = P\tilde{Y}$, becomes

$$\tilde{Y}' = \tilde{F}(\mu; \tilde{Y}), \tag{7}$$

where P is the eigenmatrix [23, 50].

Let $z_1 = y_1 + \mathrm{i}y_2$, $z_2 = \bar{z}_1$, $z_3 = y_3 + \mathrm{i}y_4$, $z_4 = \bar{z}_3$, $z = (z_1, z_2, z_3, z_4)^{\mathrm{T}}$, $G^{(1)} = \tilde{F}_1 + \mathrm{i}\tilde{F}_2 - \lambda_1 z_1$, $G^{(2)} = \tilde{F}_3 + \mathrm{i}\tilde{F}_4 - \lambda_3 z_3$, $W = (y_5, y_6, \ldots, y_{2n})^{\mathrm{T}}$, $H = (\tilde{F}_5, \tilde{F}_6, \cdots, \tilde{F}_{2n})^{\mathrm{T}} - D_1 W$, map (7) may be expressed by

$$\begin{aligned} z'_1 &= \lambda_1 z_1 + G^{(1)}(z_1, \bar{z}_1, z_3, \bar{z}_3, W; \mu), \quad z'_3 = \lambda_3 z_3 + G^{(2)}(z_1, \bar{z}_1, z_3, \bar{z}_3, W; \mu) \\ W' &= D_1 W + H(z_1, \bar{z}_1, z_3, \bar{z}_3, W; \mu) \end{aligned} \tag{8}$$

in which $\lambda_i = \tilde{\lambda}_i(\mu) = \lambda_i(v_c + \mu)$, $\tilde{\lambda}_{1,2}(0) = \alpha_1 \pm \mathrm{i}\varpi_1$, $\tilde{\lambda}_{3,4}(0) = \alpha_2 \pm \mathrm{i}\varpi_2$, $\left|\tilde{\lambda}_{1,2}(0)\right| = 1$, $\left|\tilde{\lambda}_{3,4}(0)\right| = 1$. D_1 is a real matrix of degree $(2n-4) \times (2n-4)$ with the eigenvalues $\tilde{\lambda}_5(\mu)$, $\tilde{\lambda}_6(\mu), \ldots, \tilde{\lambda}_{2n}(\mu)$.

Using the center manifold theorem technique and normal form method of maps, we can reduce map (8) to the normal form map $\Phi(z;\varepsilon)$, which is given by

$$z'_1 = \tilde{\lambda}_1(0) z_1 + \tilde{\varepsilon}_1 z_1 + \tilde{a} z_1^2 \bar{z}_1 + \tilde{b} z_1 z_3 \bar{z}_3 + O((|z_1| + |z_3|)^5),$$

$$z'_3 = \tilde{\lambda}_3(0) z_3 + \tilde{\varepsilon}_3 z_3 + \tilde{f} z_3^2 \bar{z}_3 + \tilde{e} z_1 \bar{z}_1 z_3 + O((|z_1| + |z_3|)^5). \tag{9}$$

The normal form map (9), in the real form $\Phi(Y;\varepsilon)$, is expressed by

$$\begin{aligned}
y_1' &= \alpha_1 y_1 - \varpi_1 y_2 + \varepsilon_1 y_1 - \varepsilon_2 y_2 + (ay_1 - cy_2)(y_1^2 + y_2^2) + (by_1 - dy_2)(y_3^2 + y_4^2) + h.o.t,\\
y_2' &= \alpha_1 y_2 + \varpi_1 y_1 + \varepsilon_1 y_2 + \varepsilon_2 y_1 + (ay_2 + cy_1)(y_1^2 + y_2^2) + (by_2 + dy_1)(y_3^2 + y_4^2) + h.o.t,\\
y_3' &= \alpha_2 y_3 - \varpi_2 y_4 + \varepsilon_3 y_3 - \varepsilon_4 y_4 + (fy_3 - hy_4)(y_3^2 + y_4^2) + (ey_3 - gy_4)(y_1^2 + y_2^2) + h.o.t,\\
y_4' &= \alpha_2 y_4 + \varpi_2 y_3 + \varepsilon_3 y_4 + \varepsilon_4 y_3 + (fy_4 + hy_3)(y_3^2 + y_4^2) + (ey_4 + gy_3)(y_1^2 + y_2^2) + h.o.t
\end{aligned} \tag{10}$$

in which, $\varepsilon = (\varepsilon_1, \varepsilon_2, \varepsilon_3, \varepsilon_4)^{\mathrm{T}}$, $\varepsilon_i = \varepsilon_i(\mu)$, $\varepsilon_i(0) = 0, i = 1, 2, 3, 4$.

The linearized map of $\Phi(Y;\varepsilon)$ at the fixed point is now

$$A = \left.\frac{\partial \Phi(Y,\varepsilon)}{\partial Y}\right|_{(0,\rightleftarrows\varepsilon)} = \begin{bmatrix} \alpha_1 + \varepsilon_1 & -(\varpi_1 + \varepsilon_2) & 0 & 0 \\ \varpi_1 + \varepsilon_2 & \alpha_1 + \varepsilon_1 & 0 & 0 \\ 0 & 0 & \alpha_2 + \varepsilon_3 & -(\varpi_2 + \varepsilon_4) \\ 0 & 0 & \varpi_2 + \varepsilon_4 & \alpha_2 + \varepsilon_3 \end{bmatrix}. \tag{11}$$

Ignoring the terms of high order of ε, the bifurcation boundary is given by $\alpha_1\varepsilon_1 + \varpi_1\varepsilon_2 = 0$ and $\alpha_2\varepsilon_3 + \varpi_2\varepsilon_4 = 0$. If $\alpha_1\varepsilon_1 + \varpi_1\varepsilon_2 < 0$, $\alpha_2\varepsilon_3 + \varpi_2\varepsilon_4 < 0$, the fixed point $Y_0 = (0,0,0,0)^{\mathrm{T}}$ is stable, otherwise it is unstable. On the boundary line $\alpha_1\varepsilon_1 + \varpi_1\varepsilon_2 = 0$ or $\alpha_2\varepsilon_3 + \varpi_2\varepsilon_4 = 0$, Neimark–Sacker bifurcation associated with the fixed point occurs. The direction of Neimark–Sacker bifurcation (supercritical or subcritical) depends on the high-order terms of $\Phi(Y;\varepsilon)$.

Let $\varepsilon_i = h_{i1}\mu_1 + h_{i2}\mu_2 + O(|\mu_1| + |\mu_2|)^2$, $i = 1, 2, 3, 4$. Ignoring the terms of high order of ε, the bifurcation boundary becomes

$$(\alpha_1 h_{11} + \varpi_1 h_{21})\mu_1 + (\alpha_1 h_{12} + \varpi_1 h_{22})\mu_2 = 0, \quad (\alpha_2 h_{31} + \varpi_2 h_{41})\mu_1 + (\alpha_2 h_{32} + \varpi_2 h_{42})\mu_2 = 0. \tag{12}$$

5. Local codimension two bifurcations of the normal form map

5.1. The classification of unfoldings cases

A full understanding of the normal form map (10) requires more than Jacobian matrix (11). So it is necessary to change the normal form map (10) to the polar coordinate form $\Phi(r, \theta; \varepsilon_0) \in \boldsymbol{R}^2 \times \boldsymbol{S}^2$, $(r_1, r_2, \theta_1, \theta_2) \to (r_1', r_2', \theta_1', \theta_2')$.

Let $\tilde{\varepsilon}_1 = \tilde{\lambda}_1(0)\tilde{\varepsilon}_{10}$, $\tilde{\varepsilon}_3 = \tilde{\lambda}_3(0)\tilde{\varepsilon}_{30}$, $\tilde{a} = \tilde{\lambda}_1(0)\tilde{a}_0$, $\tilde{b} = \tilde{\lambda}_1(0)\tilde{b}_0$, $\tilde{e} = \tilde{\lambda}_3(0)\tilde{e}_0$ and $\tilde{f} = \tilde{\lambda}_3(0)\tilde{f}_0$, the normal form map (9) becomes

$$\begin{aligned}
z_1' &= \tilde{\lambda}_1(0) z_1 (1 + \tilde{\varepsilon}_{10} + \tilde{a}_0 z_1 \bar{z}_1 + \tilde{b}_0 z_3 \bar{z}_3) + O((|z_1| + |z_3|)^5),\\
z_3' &= \tilde{\lambda}_3(0) z_3 (1 + \tilde{\varepsilon}_{30} + \tilde{e}_0 z_1 \bar{z}_1 + \tilde{f}_0 z_3 \bar{z}_3) + O((|z_1| + |z_3|)^5).
\end{aligned} \tag{13}$$

In polar coordinates, the map $\Phi(z;\varepsilon_0) \in \boldsymbol{R}^4$ is changed to $\Phi(r, \theta; \varepsilon_0) \in \boldsymbol{R}^2 \times \boldsymbol{S}^2$, which is given by

$$\begin{aligned}
r_1' &= r_1(1 + \varepsilon_{10} + a_0 r_1^2 + b_0 r_3^2) + h.o.t, \quad r_3' = r_3(1 + \varepsilon_{30} + e_0 r_1^2 + f_0 r_3^2) + h.o.t,\\
\theta_1' &= \theta_1 + \alpha + \varepsilon_{20} + c_0 r_1^2 + d_0 r_3^2 + h.o.t, \quad \theta_3' = \theta_3 + \beta + \varepsilon_{40} + g_0 r_1^2 + h_0 r_3^2 + h.o.t.
\end{aligned} \tag{14}$$

in which, $\varepsilon_{10} = \varepsilon_1\alpha_1 + \varepsilon_2\varpi_1$, $\varepsilon_{20} = \varepsilon_2\alpha_1 - \varepsilon_1\varpi_1$, $\varepsilon_{30} = \varepsilon_3\alpha_2 + \varepsilon_4\varpi_2$ and $\varepsilon_{40} = \varepsilon_4\alpha_2 - \varepsilon_3\varpi_2$ are the unfolding parameters, and $\varepsilon_0 = (\varepsilon_{10}, \varepsilon_{30})^{\mathrm{T}}$; $a_0 = a\alpha_1 + c\varpi_1$, $c_0 = c\alpha_1 - a\varpi_1$, $b_0 = b\alpha_1 + d\varpi_1$, $d_0 = d\alpha_1 - b\varpi_1$, $e_0 = e\alpha_2 + g\varpi_2$, $g_0 = g\alpha_2 - e\varpi_2$, $f_0 = f\alpha_2 + h\varpi_2$, $h_0 = h\alpha_2 - f\varpi_2$.

We can deduce much of the behavior of this system by ignoring the azimuthal components. In this way, a two-dimensional map is obtained, which is now

$$r_1' = r_1(1 + \varepsilon_{10} + a_0 r_1^2 + b_0 r_3^2) + h.o.t, \quad r_3' = r_3(1 + \varepsilon_{30} + e_0 r_1^2 + f_0 r_3^2) + h.o.t. \tag{15}$$

Letting $\bar{r}_1 = r_1\sqrt{|a_0|}$and $\bar{r}_3 = r_3\sqrt{|f_0|}$, we obtain the following:

$$\bar{r'}_1 = \bar{r}_1(1 + \varepsilon_{10} + \bar{r}_1^2 + \bar{b}\bar{r}_3^2) + h.o.t, \quad \bar{r'}_3 = \bar{r}_3(1 + \varepsilon_{30} + \bar{c}\bar{r}_1^2 + \bar{d}\bar{r}_3^2) + h.o.t, \tag{16}$$

where $\bar{b} = b_0/|f_0|$, $\bar{c} = e_0/|a_0|$ and $\bar{d} = \pm 1$.

For convenience in the following, we drop the bar of these symbols $\bar{b}$, $\bar{c}$ and $\bar{d}$, and use still b, c and d instead of $\bar{b}$, $\bar{c}$ and $\bar{d}$, respectively.

Map (16) can be represented for all sufficiently small $\|\varepsilon_0\|$ in the form

$$\bar{R} \mapsto \varphi^1_{\varepsilon_0}(\bar{R}) + O(\|\bar{R}\|^4),$$

where $\bar{R} = (\bar{r}_1, \bar{r}_2)^{\mathrm{T}}$, $\varphi^t_{\varepsilon_0}$ is the flow of a planar system, that is smoothly equivalent to the system [45,46]

$$\dot{\rho}_1 = \rho_1(\varepsilon_{10} + \rho_1^2 + b\rho_3^2) + h.o.t, \quad \dot{\rho}_3 = \rho_3(\varepsilon_{30} + c\rho_1^2 + d\rho_3^2) + h.o.t. \tag{17}$$

Now consider bifurcations and parameter unfoldings of the approximating system (17). The 3-jet of (17) with $\varepsilon_{10} = \varepsilon_{30} = 0$ is determined (with respect to suitably symmetric higher-order perturbations). Provided that a_0, b_0, e_0, f_0 are not equal to zero and $a_0f_0 - b_0e_0 \neq 0$ implying that $d - bc \neq 0$ in Eq. (17). Nine topologically distinct equivalence classes are shown in Fig. 2 and Table 1. It is to be noted that $2c$ and $2e$, $2d$ and $2f$, respectively, are topologically equivalent if we allow reversal of time and reflection about the diagonal in invariant line.

In particular, we note that invariant radial lines $\rho_3 = \sqrt{(1-c)(d-b)}\rho_1$ exist whenever $(1-c)(d-b) > 0$, but we do not distinguish between phase portraits which are equivalent up to reversal of time. In Fig. 2, only the positive (ρ_1, ρ_3) quadrant is shown. Since the phase portraits are symmetric under reflection about both axes. Fig. 2 should be read in conjunction with Table 1.

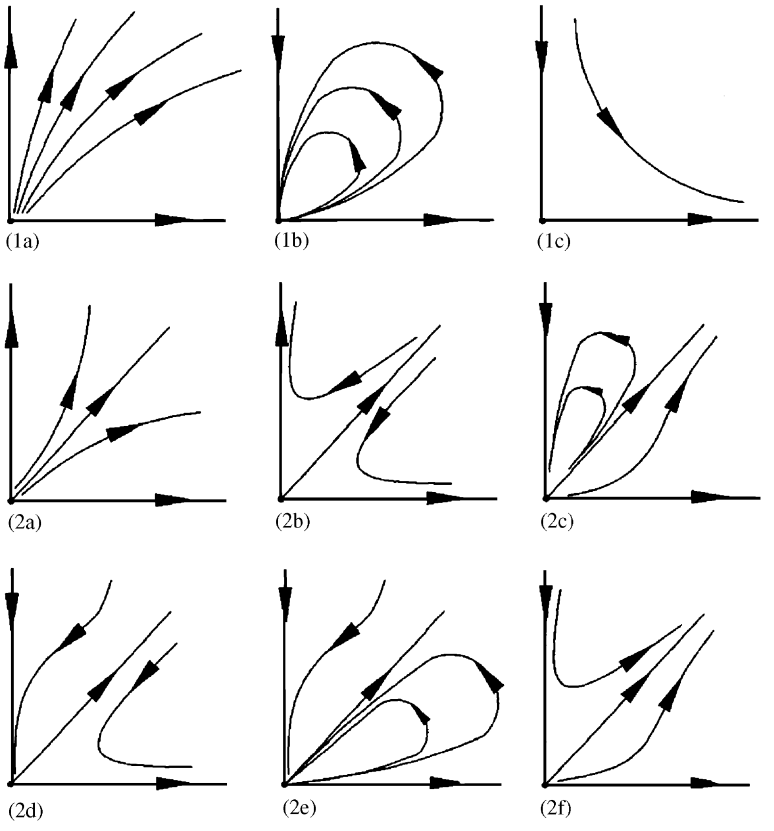

Fig. 2. Nine phase portraits for the degenerate vector field.

Table 1
The nine degenerate fixed points

Type 1: two invariant lines:$(1-c)(d-b)<0$
1a: $d=+1$, all appropriate b, c
1b: $d=-1$, $c>0>b$, $-1-bc>0$
1c: $d=-1$, all other b, c
Type 2: three invariant lines:$(1-c)(d-b)>0$
2a: $d=+1$, $(1-bc)(1-b)>0$, all appropriate b, c
2b: $d=+1$, $(1-bc)(1-b)<0$, all appropriate b, c
2c: $d=-1$, $(-1-bc)(-1-b)>0$, $b<-1$, $c<1$
2d: $d=-1$, $(-1-bc)(-1-b)<0$, $b<-1$, $c>1$
2e: $d=-1$, $(-1-bc)(-1-b)<0$, $b>-1$, $c<1$
2f: $d=-1$, $(-1-bc)(-1-b)>0$, $b>-1$, $c<1$

Table 2
The 12 unfoldings

Case	1(a)	1(b)	2	3	4(a)	4(b)	5	6(a)	6(b)	7(a)	7(b)	8
d	$+1$	$+1$	$+1$	$+1$	$+1$	$+1$	-1	-1	-1	-1	-1	-1
b	$+$	$+$	$+$	$-$	$-$	$-$	$+$	$+$	$+$	$-$	$-$	$-$
c	$+$	$+$	$-$	$+$	$-$	$-$	$+$	$-$	$-$	$+$	$+$	$-$
$d-bc$	$+$	$-$	$+$	$+$	$+$	$-$	$-$	$+$	$-$	$+$	$-$	$-$

The classification of degenerate fixed points given above is not the most natural when it comes to studying the unfoldings. Here there are 12 distinct cases. As set out in Table 2.

The present classification is based on a study of secondary pitchfork bifurcations from nontrivial equilibria for the planar vector field. We note that $Y_0^*=(0,0)^{\mathrm{T}}$ is always an equilibrium and that up to three other equilibria (in the positive quadrant) can appear. As follows:

$$Y_1^*=(\sqrt{-\varepsilon_{10}},0)^{\mathrm{T}},\quad \text{for}\quad \varepsilon_{10}<0;\quad Y_2^*=(0,\sqrt{-\varepsilon_{30}/d})^{\mathrm{T}}\quad \text{for}\quad \varepsilon_{30}/d<0,$$
$$Y_3^*=\left(\sqrt{\frac{b\varepsilon_{30}-d\varepsilon_{10}}{d-bc}},\sqrt{\frac{c\varepsilon_{10}-\varepsilon_{30}}{d-bc}}\right)^{\mathrm{T}}\quad \text{for}\quad \frac{b\varepsilon_{30}-d\varepsilon_{10}}{d-bc}>0,\quad \frac{c\varepsilon_{10}-\varepsilon_{30}}{d-bc}>0. \tag{18}$$

Pitchfork bifurcation occurs from $Y_0^*=(0,0)^{\mathrm{T}}$ on the lines $\varepsilon_{10}=0$ and $\varepsilon_{30}=0$, and also Pitchfork bifurcation occurs from $Y_1^*=(\sqrt{-\varepsilon_{10}},0)^{\mathrm{T}}$ on the line $\varepsilon_{30}=c\varepsilon_{10}$, and from $Y_2^*=\left(0,\sqrt{-\varepsilon_{30}/d}\right)^{\mathrm{T}}$ on the line $\varepsilon_{30}=d\varepsilon_{10}/b$. The stability types of these bifurcations are determined by Jacobian matrix associated with corresponding fixed point.

The behavior remains relatively simple as long as Hopf bifurcations do not occur from the fixed point $Y_3^*=(\bar{\rho}_1,\bar{\rho}_3)^{\mathrm{T}}=(\sqrt{(b\varepsilon_{30}-d\varepsilon_{10})/(d-bc)},\sqrt{(c\varepsilon_{10}-\varepsilon_{30})/(d-bc)})^{\mathrm{T}}$. To detect such bifurcations, we linearize at this fixed point to obtain the matrix

$$A=\begin{bmatrix}\varepsilon_{10}+3\bar{\rho}_1^2+b\bar{\rho}_3^2 & 2b\bar{\rho}_1\bar{\rho}_3\\ 2c\bar{\rho}_1\bar{\rho}_3 & \varepsilon_{30}+c\bar{\rho}_1^2+3d\bar{\rho}_3^2\end{bmatrix}. \tag{19}$$

Hopf bifurcations of this fixed point can occur only on the line

$$\varepsilon_{30}=\frac{\varepsilon_{10}d(1-c)}{b-d}, \tag{20}$$

when $d-bc>0$, we immediately see that Hopf bifurcation cannot occur in cases 1(b), 4(b), 5, 6(b), 7(b) and 8. It is also easy to show that they cannot occur in cases 1(a), 2, 3 and 4(a), since for such bifurcations to occur,

the slope $d(1-c)/(b-d)$ of the line given by (20) must lie between the slopes of the pitchfork lines

$$L_{s1}: \quad \varepsilon_{30} = c\varepsilon_{10} \quad \text{and} \quad L_{s2}: \varepsilon_{30} = \frac{d\varepsilon_{10}}{b},$$

and in the appropriate sector of the $(\varepsilon_{10}, \varepsilon_{30})$ plane. In each of these four cases, simple computations reveal that this requirement contradicts the condition $d - bc > 0$. Therefore Hopf bifurcation can occur only in cases 6(a), 7(a).

5.2. The bifurcation sets and phase portraits for the unfoldings for cases 1, 2, 3, 4, 5, 6(b), 7(b), and 8

$Y_0^* = (0,0)^{\mathrm{T}}$is trivial equilibrium, the condition for local stability is $\varepsilon_{10} < 0$ and $\varepsilon_{30} < 0$. The condition for existence of $Y_1^* = \left(\sqrt{-\varepsilon_{10}}, 0\right)^{\mathrm{T}}$ is $\varepsilon_{10} < 0$, the condition for local stability is $\varepsilon_{10} > 0$, $\varepsilon_{30} < c\varepsilon_{10}$. The condition for existence of $Y_2^* = \left(0, \sqrt{-\varepsilon_{30}/d}\right)^{\mathrm{T}}$ is $\varepsilon_{30}/d < 0$, the condition for local stability is $\varepsilon_{30} > 0$, $\varepsilon_{10} < b\varepsilon_{30}/d$. Accordingly we have the following unfoldings, the bounds of the region shown in Figs. 3–7 in following ten cases can mostly be listed as follows:

$$L_{s1}: \quad \varepsilon_{30} = c\varepsilon_{10} \quad \text{and} \quad L_{s2}: \quad \varepsilon_{30} = \frac{d\varepsilon_{10}}{b}.$$

5.3. The bifurcation sets and phase portraits for the unfoldings for cases 6(a) and 7(a)

The condition for existence of $Y_3^* = (\sqrt{(b\varepsilon_{30} - d\varepsilon_{10})/(d-bc)}, \sqrt{(c\varepsilon_{10} - \varepsilon_{30})/(d-bc)})^{\mathrm{T}}$ is $(b\varepsilon_{30} - d\varepsilon_{10})/(d-bc) > 0$ and $c\varepsilon_{10} - \varepsilon_{30}/d - bc > 0$, the condition for local stability is determined by the analysis in the eigenvalues of relevant Jacobian matrix (19). Hopf bifurcations associated the fixed point can occur only on the line

$$\varepsilon_{30} = \frac{\varepsilon_{10} d(1-c)}{b-d}.$$

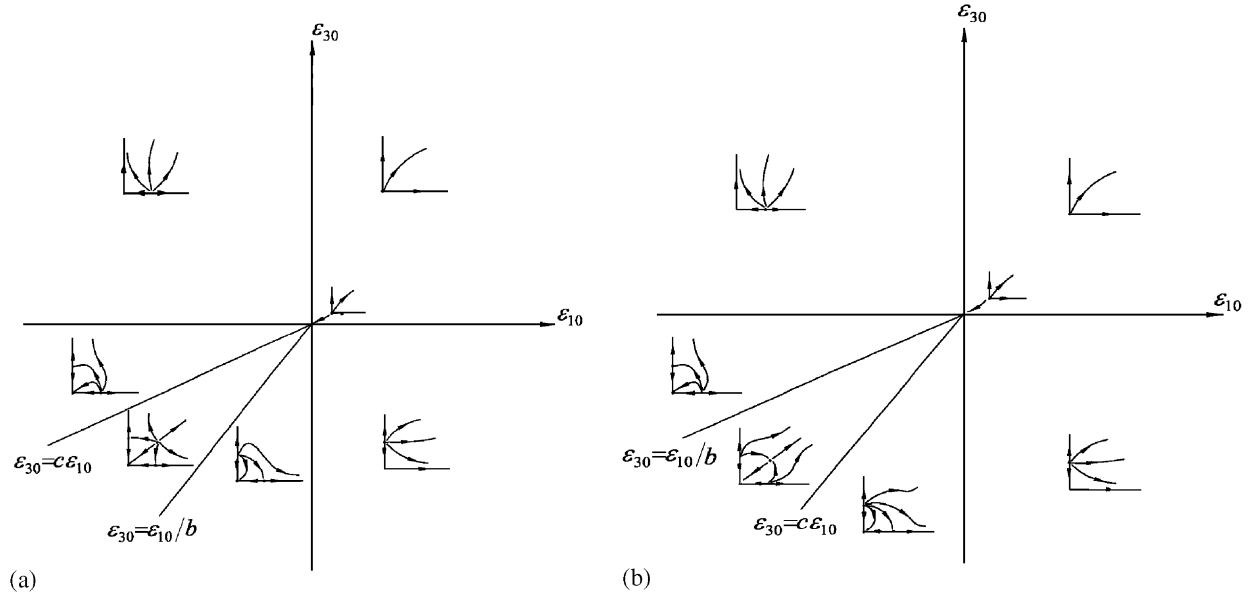

Fig. 3. The unfoldings for cases 1(a) and (b) (cf. degenerate types 1a, 2a).

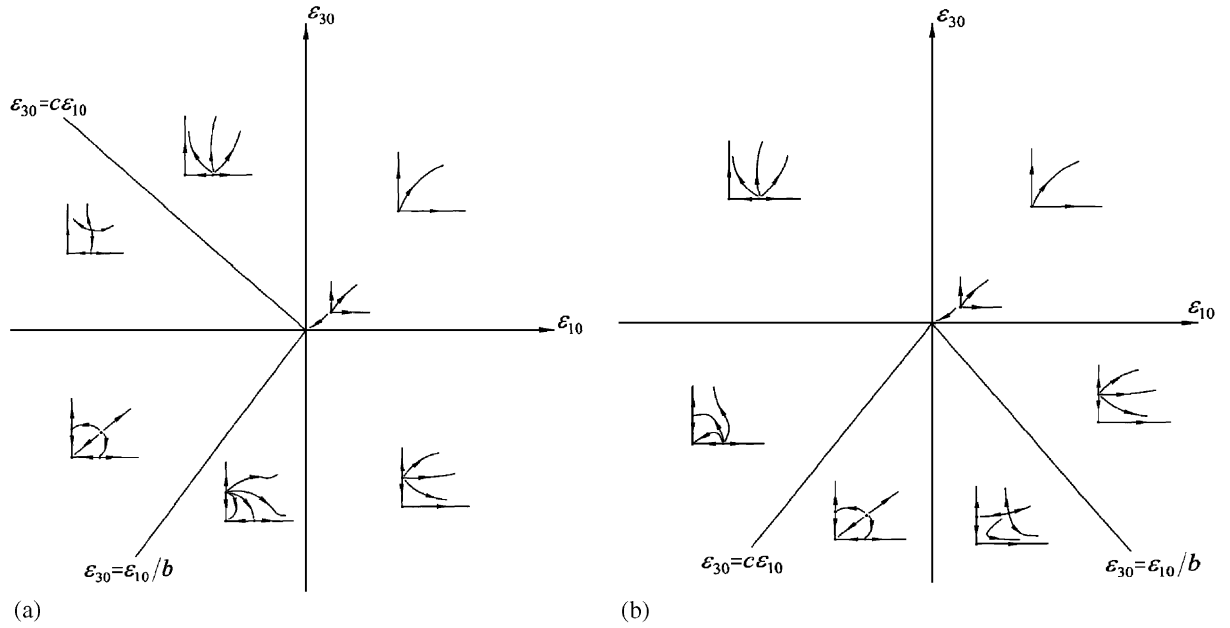

Fig. 4. The unfoldings for cases 2 and 3 (cf. degenerate types 1a, 2a).

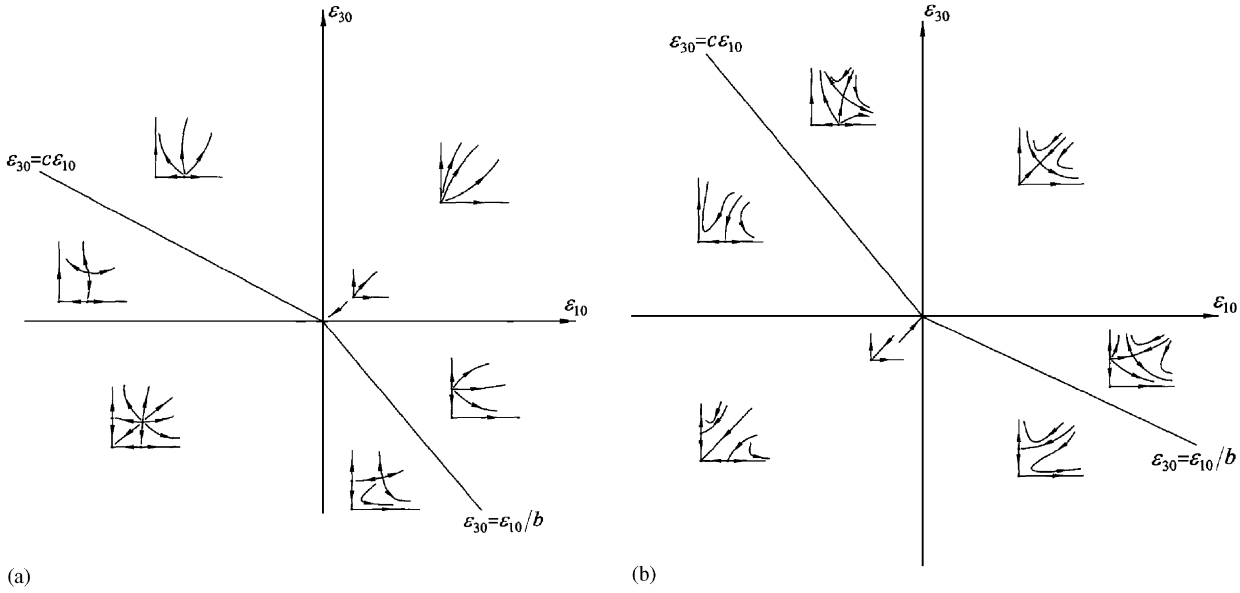

Fig. 5. The unfoldings for cases 4(a) and (b) (cf. degenerate types 1a, 2a, and 2b, respectively).

5.3.1. The bifurcation sets and phase portraits for the unfolding for case 6(a)

For the case $d=-1$, $b>0$, $c<0$, $d-bc<0$, the local stable conditions of the equilibrium Y_3^* is $\varepsilon_{10}<0$, $\varepsilon_{30}>d\varepsilon_1/b$, $\varepsilon_{30}<\varepsilon_{10}d(1-c)/(b-d)$. The partial bifurcation set and phase portraits for unfolding associated the case are shown in Fig. 8. The bounds of all regions shown in Fig. 8 can be listed as follows:

$$L_1: \quad \varepsilon_{30}=0, \quad \varepsilon_{10}<0, \quad L_2: \quad \varepsilon_{30}=\frac{d}{b}\varepsilon_{10}, \quad \varepsilon_{10}<0, \quad L_3: \quad \varepsilon_{30}=\frac{\varepsilon_{10}d(1-c)}{b-d}$$
$$\varepsilon_{10}<0, \quad L_4: \quad \varepsilon_{30}=c\varepsilon_{10}, \quad \varepsilon_{10}<0, \quad L_5: \varepsilon_{10}=0, \quad \varepsilon_{30}<0.$$

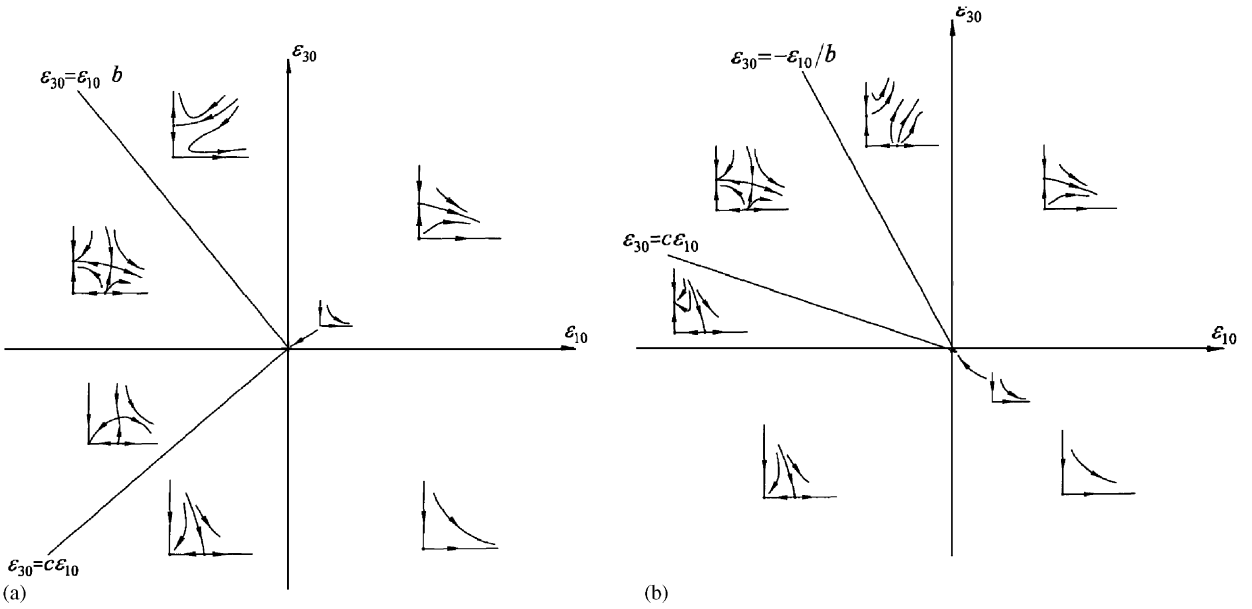

Fig. 6. The unfoldings for cases 5 and 6(b) (cf. degenerate type 1c).

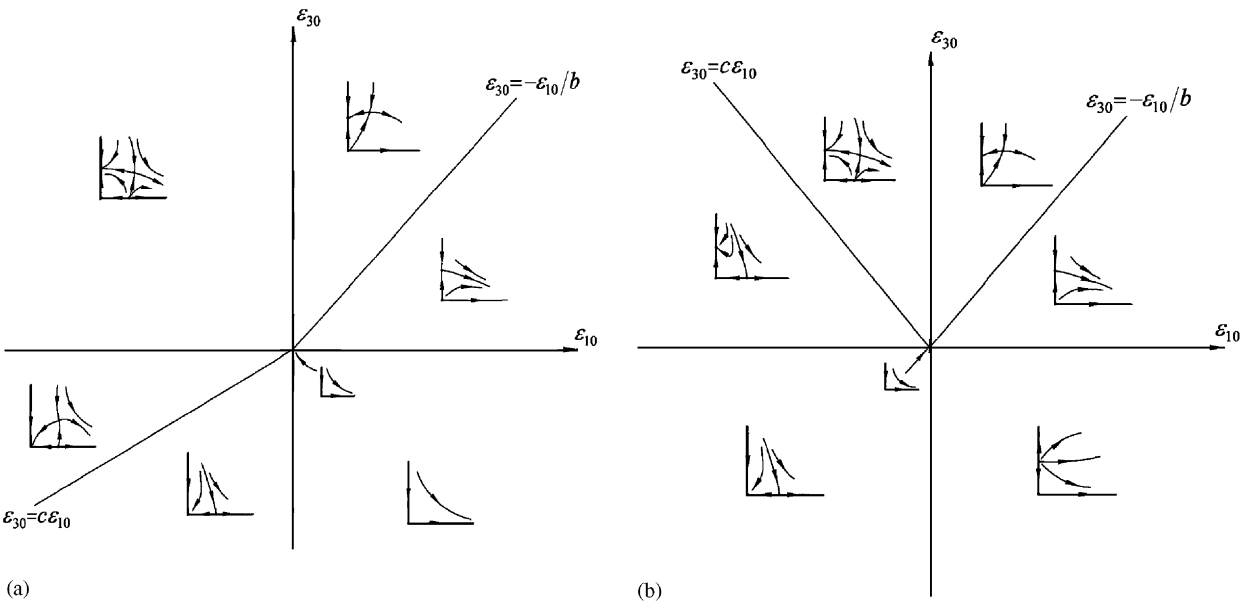

Fig. 7. The unfoldings for cases 7(b) and 8 (cf. degenerate type 1c).

Now consider the case 6(a), in which a Hopf bifurcation can occur. For this case, we obtain the partial bifurcation set and phase portraits of Fig. 8. On the Hopf bifurcation line given by formula (20) we find that the system

$$\dot{\rho}_1 = \rho_1(\varepsilon_{10} + \rho_1^2 + b\rho_3^2) + h.o.t, \quad \dot{\rho}_3 = \rho_3\left(\varepsilon_{10}\left(\frac{c-1}{b+1}\right) + c\rho_1^2 - \rho_3^2\right) + h.o.t, \tag{21}$$

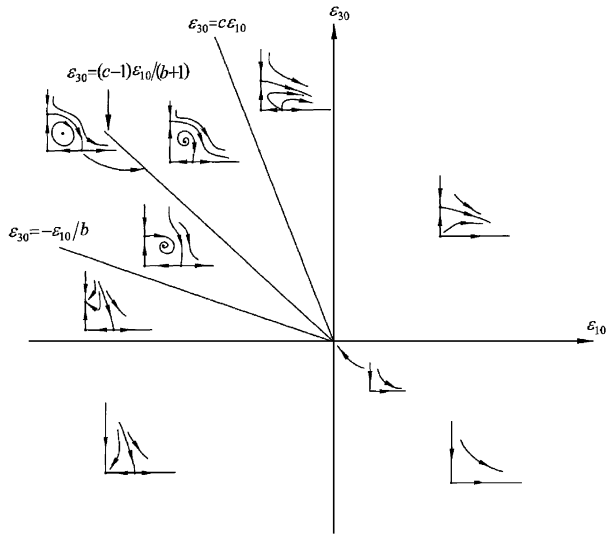

Fig. 8. Partial bifurcation set and phase portraits for the unfolding of case 6(a).

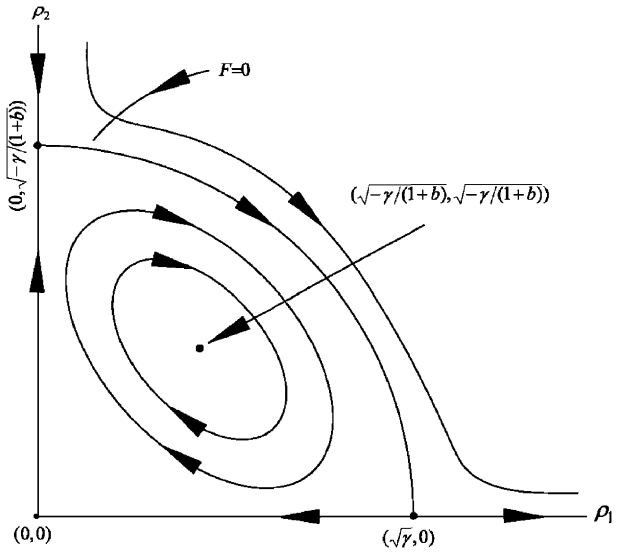

Fig. 9. Level curves of $F(\rho_1,\rho_2)$ for case 6(a) ($b>0$, $c>0$).

is integrable, and that the function

$$F(\rho_1,\rho_3)=\rho_1^{\alpha}\rho_3^{\beta}(\varepsilon_{10}+(\rho_1^2+\eta\rho_3^2)),\quad \dot{\rho}_3=\rho_3\left(\varepsilon_{10}\left(\frac{c-1}{b+1}\right)+c\rho_1^2-\rho_3^2\right)+h.o.t, \tag{22}$$

where $\alpha=2(1-c)/A$, $\beta=2(1+b)/A$, and $\eta=(1+b)/(1-c)$, is constant along solution curves. In case 6(a), $b>0>c$, $A=-1-bc>0$ and $\mu_1\overset{\text{Def}}{=}-\gamma<0$, and the level curves of this function take the form shown in Fig. 9.

Once more it is necessary to add higher-order terms to "stabilize" the degenerate Hopf bifurcation and to determine the topological type of this unfoldings. In the case the terms are homogeneous of fifth order:

$$\rho_1(\bar{e}\rho_1^4+\bar{f}\rho_1^2\rho_3^2+\bar{g}\rho_3^4),\quad \rho_3(h\rho_1^4+j\rho_1^2\rho_3^2+k\rho_3^4). \tag{23}$$

Adding these quintic terms to the original Eq. (17) with $d=-1$, using the transformations

$$\rho_1=\sqrt{\varepsilon}u,\quad \rho_3=\sqrt{\varepsilon}v,\quad \varepsilon_{10}=\varepsilon v_1,\quad \varepsilon_{30}=\varepsilon v_1\left(\frac{c-1}{b+1}\right)+\varepsilon^2 v_2 \tag{24}$$

and rescaling time $t\to\varepsilon t$, we obtain

$$\begin{aligned}\dot{u}&=u(v_1+u^2+bv^2)+\varepsilon u(\bar{e}u^4+\bar{f}u^2v^2+\bar{g}v^4),\\ \dot{v}&=v\left(v_1\left(\frac{c-1}{b+1}\right)+cu^2-v^2\right)+\varepsilon v(v_2+hu^4+ju^2v^2+kv^4).\end{aligned} \tag{25}$$

We again have to study a small perturbation of an integrable system. Multiplying (25) by the integrating factor $u^{\alpha-1}v^{\beta-1}$, we obtain the "equivalent" perturbed Hamiltonian system:

$$\begin{aligned}\dot{u}&=u^{\alpha}v^{\beta-1}[(v_1+u^2+bv^2)+\varepsilon(\bar{e}u^4+\bar{f}u^2v^2+\bar{g}v^4)],\\ \dot{v}&=u^{\alpha-1}v^{\beta}\left[\left(v_1\left(\frac{c-1}{b+1}\right)+cu^2-v^2\right)+\varepsilon(v_2+hu^4+ju^2v^2+kv^4)\right].\end{aligned} \tag{26}$$

The Hamiltonian function for (26) is

$$F(u,v)=\frac{1}{\beta}u^{\alpha}v^{\beta}\left(v_1+\left(u^2+\left(\frac{1+b}{1-c}\right)v^2\right)\right), \tag{27}$$

where $\alpha=2(1-c)/A$, $\beta=2(1+b)/A$, $A=-1-bc>0$.

In studying case 6(a), we can set $v_1=-1$ without loss of generality.

Denoting such a curve $F(u,v)=K$ by Γ_k. We require that the function

$$\iint_{\mathrm{int}\Gamma_k}\{\beta v_2+[(\alpha+4)\bar{e}+\beta h]u^4+[(\alpha+2)\bar{f}+(\beta+2)j]u^2v^2+[\alpha\bar{g}+(\beta+4)k]v^4\}u^{\alpha-1}v^{\beta-1}\,\mathrm{d}u\,\mathrm{d}v \tag{28}$$

has simple zeros with respect to variation of the parameter v_2 and the coefficients $\bar{e}$, $\bar{f}$, $\bar{g}$, h, j, k, Writing the four integrals of (28) as $I_j(K)$, we therefore require

$$v_2=-\frac{1}{\beta I_1(K)}[BI_2(K)+CI_3(K)+DI_4(K)], \tag{29}$$

where $B=(\alpha+4)e+\beta h$, $C=(\alpha+2)f+(\beta+2)j$ and $D=\alpha g+(\beta+4)k$.

On the homoclinic loop we have $F=0$ and can thus use the substitution

$$u^2+\left(\frac{1+b}{1-c}\right)v^2=1.$$

Letting $(1-c)/(1+b)=M$, $v^2=M(1-u^2)$, we obtain

$$v_2=-\frac{1}{\beta I_1(0)}[BI_2(0)+CI_3(0)+DI_4(0)],$$

where $I_1(0)=(M^{\beta/2}/\beta)\int_0^1 u^{\alpha-1}(1-u^2)^{\beta/2}\,\mathrm{d}u$, $I_2(0)=(M^{\beta/2}/\beta)\int_0^1 u^{\alpha+3}(1-u^2)^{\beta/2}\,\mathrm{d}u$, $I_3(0)=(M^{(\beta+2)/2}/(\beta+2))\int_0^1 u^{\alpha+1}(1-u^2)^{(\beta+2)/2}\,\mathrm{d}u$, $I_4(0)=(M^{(\beta+4)/2}/\beta+4))\int_0^1 u^{\alpha-1}(1-u^2)^{(\beta+4)/2}\,\mathrm{d}u$.

We therefore have the bifurcation set

$$\varepsilon_{30}=\frac{c-1}{b+1}\varepsilon_{10}-\frac{\varepsilon_{10}^2}{\beta I_1(0)}[BI_2(0)+CI_3(0)+DI_4(0)]. \tag{30}$$

On the basis of the discussion above, in Fig. 10 we sketch two possible completions of the unfolding of case 6(a) (for $M>0$). The vector fields in the remaining sectors are as in Fig. 8. In Fig. 10(b) two bifurcation curves exist on which periodic orbits coalesce in saddle-node bifurcation.

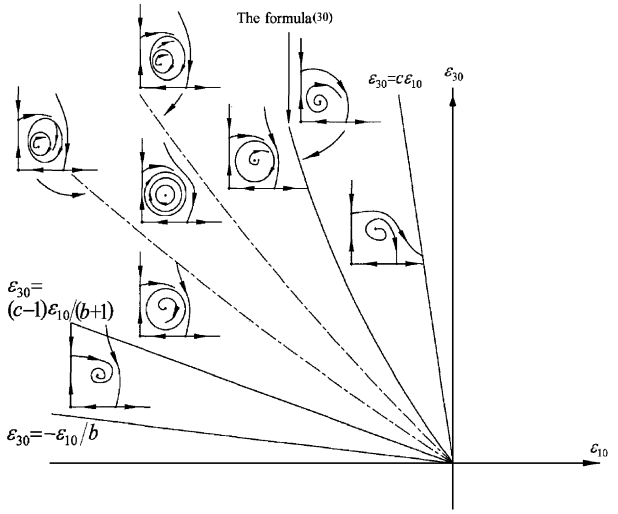

Fig. 10. Possible completions of the unfolding of case 6(a) (The two coalescences of periodic orbits).

5.3.2. The bifurcation sets and phase portraits for the unfolding for case 7(a)

The remaining case, 7a is even more complicated than the one we have just outlined, since it really contains three distinct subcases, depending upon the relative sizes of the coefficients b and c. These determine whether the Hopf bifurcation line lies in the first, third, or fourth quadrants. The three cases are shown in Fig. 11, and represent unfoldings of the degenerate types 2e, 1b, and 2c (see Table 1), respectively. The first integral $F(\rho_1, \rho_3)$ of (16) is invariant on solution curves in all these cases when

$$\varepsilon_{30} = \varepsilon_{10}\left(\frac{c-1}{b+1}\right)$$

(i.e., on the Hopf bifurcation line). However, we note that in these cases at least one of the indices α, β is always negative and thus that the integral is singular at $(\bar{\rho}_1, \bar{\rho}_3) = (0, 0)$. This fact leads to the bunching of level curves consistent with the existence of a sink or a source at $(0, 0)$.

According to the unfoldings for cases list in Table 2, the bifurcation sets of approximating system (18), near $\varepsilon_0 = (0, 0)^{\mathrm{T}}$, can approximately be illustrated by Figs. 3–11 [45,46]. Recall now that the map $\varphi^1_{\varepsilon_0}(\bar{R})$ approximates the simplified map (17), and consider the influence of azimuthal components to the map (17). We can now interpret the obtained results, first in terms of the approximating map $\varphi^1_{\varepsilon_0}(\bar{R})$, and second in terms of the normal form map. For the normal form map $\Phi(Z, \varepsilon)$, the equilibrium $Y_0^* = (0, 0)^{\mathrm{T}}$of approximating system (18) become the trivial fixed point placed at the origin; the pitchfork bifurcation of equilibrium $Y_0^* = (0, 0)^{\mathrm{T}}$ turn into the Neimark–Sacker bifurcations of the fixed point Y_0 of the normal form map, note that the direction of Neimark–Sacker bifurcation (supercritical or subcritical) depends on the high order terms of the normal form map, since the equilibria $Y_1^* = (\sqrt{-\varepsilon_{10}}, 0)^{\mathrm{T}}$ (or $Y_2^* = (0, \sqrt{-\varepsilon_{30}/d})^{\mathrm{T}}$) become closed invariant curves of corresponding stability. In the discussion above, we have found that at least one of two Neimark–Sacker bifurcations associated with the trivial fixed point on lines $\varepsilon_{10} = 0$ $(\alpha_1\varepsilon_1 + \varpi_1\varepsilon_2 = 0)$ and $\varepsilon_{30} = 0$ $(\alpha_2\varepsilon_3 + \varpi_2\varepsilon_4 = 0)$ is subcritical for the normal form map, and that supercritical Neimark–Sacker bifurcation associated the trivial fixed point occurs only in cases 5–8. The Pitchfork bifurcation of the equilibrium $Y_2^* = (0, \sqrt{-\varepsilon_{30}/d})^{\mathrm{T}}$ (or $Y_1^* = (\sqrt{-\varepsilon_{10}}, 0)^{\mathrm{T}}$) in cases 6 and 7 corresponds to instability and torus bifurcation of closed invariant curve of the map, and Hopf bifurcation of the equilibrium Y_3^* in cases 6(a) and 7(a) corresponds to the further torus bifurcation of the normal form map, both lead to the "tire-like" quasi-periodic attractor. It is to be noted that only in cases 6(a) and 7(a) the attracting quasi-periodic orbits of "tire-like" are generated.

According to the center manifold theory, local behavior of map $\tilde{f}(v, X)$, near the point v_c of double Neimark–Sacker bifurcation, is equivalent to that of the normal form $\Phi(Z; \varepsilon)$ for ε in some neighborhood of

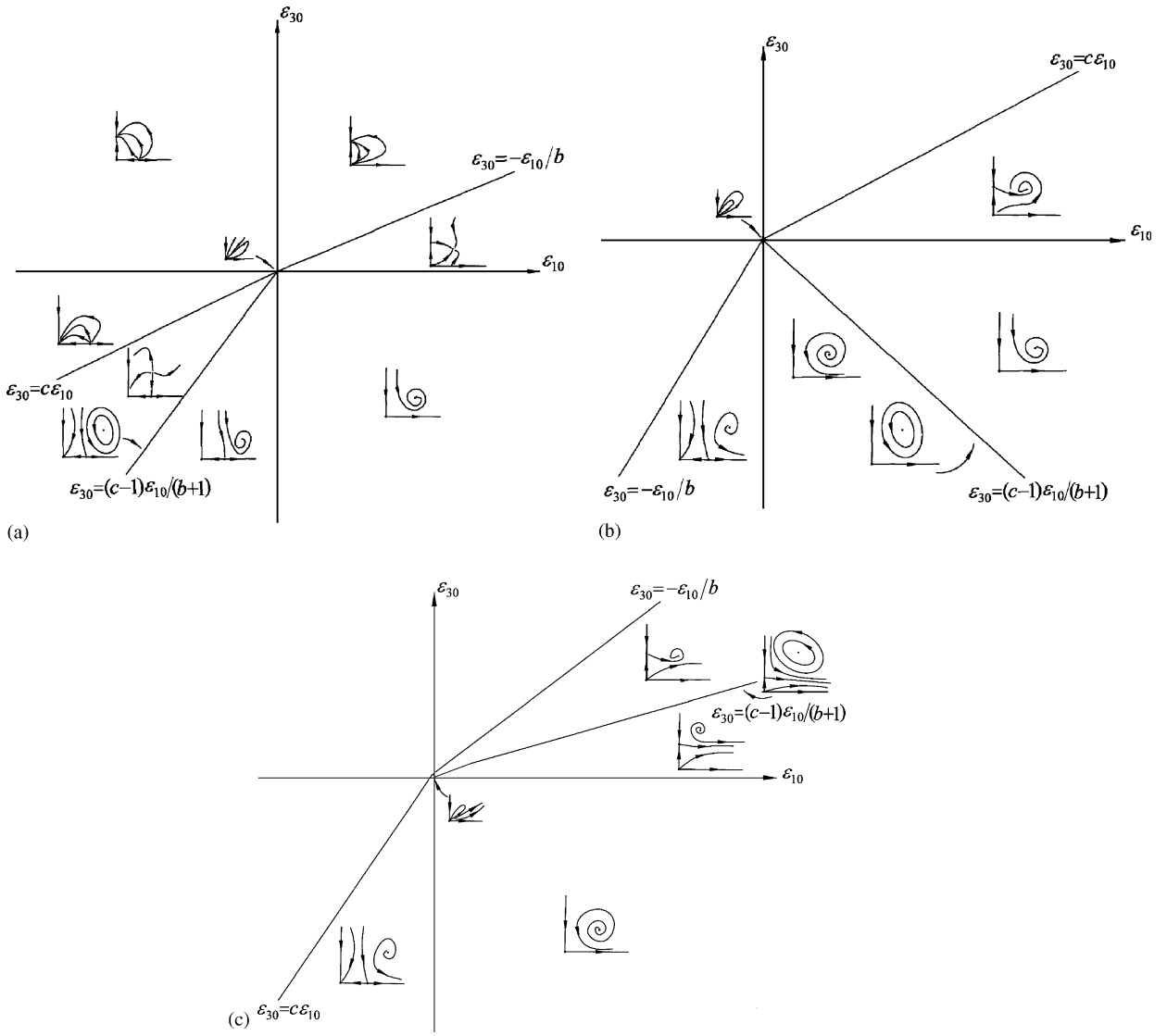

Fig. 11. Three subcases for case 7(a) (cf. degenerate cases associated with types 2e, 1b, and 2c, respectively): (a) $b>-1$, $c>1$; (b) $b>-1$, $c<1$ or $b<-1$, $c>1$; (c) $b<-1$, $c<1$.

a critical value $\varepsilon=(0,0,0,0)^{\mathrm{T}}$. By comparison with of local bifurcation behavior of the simplified map (17), we can find out dynamical behavior of the vibro-impact system in the case of double Neimark–Sacker bifurcation. By virtue of Figs. 8, 10 and 11, we can conclude that the vibro-impact system, near the value of double Neimark–Sacker bifurcation, undergoes not only Neimark–Sacker bifurcation associated with period-one double-impact symmetrical motion, but also does possibly torus bifurcation. The torus bifurcation leads to "tire-like" quasi-periodic attractor in Poincaré section. This conclusion conforms to the examples undermentioned.

6. Numerical analyses

The local stability analysis, discussed in the previous section, can reveal different kinds of bifurcations of 1-1-1 symmetrical motions namely Neimark–Sacker bifurcation, codimension two bifurcation and torus bifurcation, etc. In this section, the analysis developed in the former section is verified by the presentation of

results for the three-degree-of-freedom vibratory system shown in Fig. 12. The existence and stability of period-one double-impact symmetrical motion are analyzed explicitly. Also, local bifurcations at the points of change in stability, discussed in the previous section, are considered, thus giving some information on dynamical behavior near the point of double Neimark–Sacker bifurcation.

The system with parameters (1): $m_2 = 0.8$, $m_3 = 1.2$, $k_2 = 1.5$, $k_3 = 1.5$, $f_{10} = 0$, $f_{20} = 1$, $f_{30} = 0$, $\delta = 0.3$ and $R = 0.8$ has been chosen for analyzing its dynamical behavior near the point of double Neimark–Sacker bifurcation. The forcing frequency ω and parameter γ are taken as the control parameters, i.e. $v = (\gamma, \omega)^{\mathrm{T}}$. The eigenvalues of Jacobian matrix $Df(v, 0)$ are computed with $\omega \in [3.1, 3.195]$ and $\gamma \in [0.058, 0.065]$. The moduli of all eigenvalues of $Df(v, 0)$ are less than one for $v = (0.065, 3.195)^{\mathrm{T}}$. By gradually decreasing γ and ω from the point $v = (0.065, 3.195)^{\mathrm{T}}$ to change the control parameter v, we can obtain two complex conjugate pairs of eigenvalues $\lambda_{1,2}(v_c) = -0.5491035 \pm 0.8357545i$ $(|\lambda_{1,2}(v_c)| = 1.0)$ and $\lambda_{3,4}(v_c) = -0.9890127 \pm 0.1478241i$ $(|\lambda_{3,4}(v_c)| = 0.999999)$ which are very close to the unit circle, and the other eigenvalues $(\lambda_{5,6}(v_c) = -0.2564126 \pm 0.1354285i,\ |\lambda_{5,6}(v_c)| = 0.2899798)$ still stay inside the unit circle as v equals $v_c = (0.060153,\ 3.162899)^{\mathrm{T}}$. The eigenvalues $\lambda_{1,2}(v)$ and $\lambda_{3,4}(v)$ have escaped the unit circle as γ and ω pass through decreasingly $v = (0.060151,\ 3.1628988)^{\mathrm{T}}$. The eigenvalues $\lambda_{1,2}(v)$ and $\lambda_{3,4}(v)$ almost escape the unit circle simultaneously, so $v_c = (0.060153,\ 3.162899)^{\mathrm{T}}$ is approximately taken as the value of double Neimark–Sacker bifurcation. Using the center manifold theorem technique and normal form method of maps, we can reduce map (5) to the normal form map (10), and correspondingly obtain the analytical expression of the bifurcation parameters transformed $\varepsilon_i = h_{i1}\mu_1 + h_{i2}\mu_2 + O(|\mu_1| + |\mu_2|)^2$. For the system

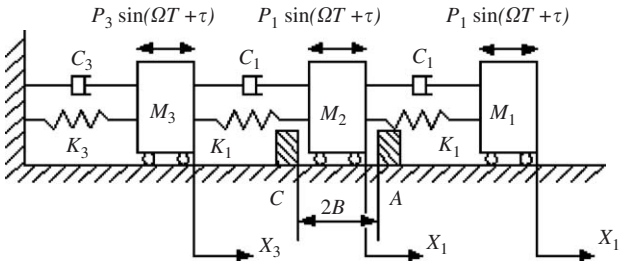

Fig. 12. Schematic of the vibratory system with symmetrical rigid stops.

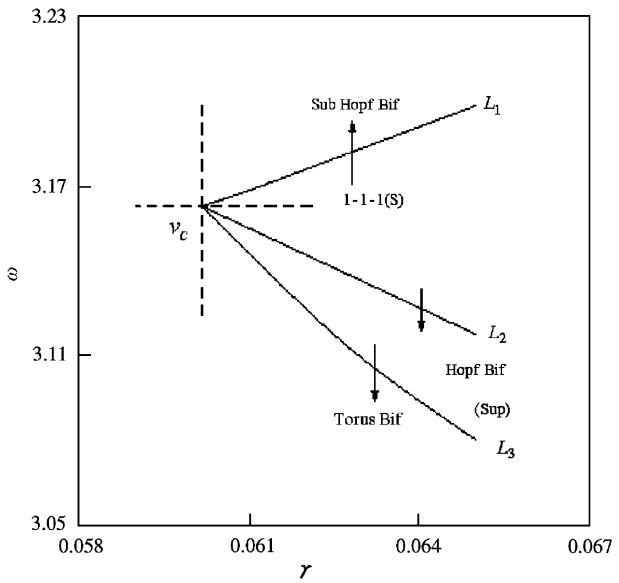

Fig. 13. The partial bifurcation set near the point of double Neimark–Sacker bifurcation.

shown in Fig. 12, with system parameters (1), the coefficients of the formula $\varepsilon_i = h_{i1}\mu_1 + h_{i2}\mu_2 + O(|\mu_1| + |\mu_2|)^2$ are

$$h_{11} = 3.864573, \quad h_{12} = -1.135826, \quad h_{21} = -5.729431, \quad h_{22} = -1.627221,$$
$$h_{31} = 1.083245, \quad h_{32} = -1.146872, \quad h_{41} = -2.008334; \quad h_{42} = -6.423976.$$

By formula (12), two lines $\mu_2 = 7.409717\mu_1$ and $\mu_2 = -9.385739\mu_1$, associated with Neimark–Sacker bifurcation of period-one double-impact symmetrical motion, can be determined. We can see that these two lines are very close to the lines L_1 and L_2 which are obtained by numerical computation and shown in Fig. 13. The lines L_1 and L_2 are obtained by computing the eigenvalues of Jacobian matrix(6) associated with the fixed points in the region of 1-1-1(S). On the lines L_1 and L_2 a complex conjugate pair of eigenvalues of Jacobian matrix(6) lie on the unit circle, the remainder of the spectrum still stay inside the unit circle. Approximate points of torus bifurcations can be obtained by computing the points of change in stability of attracting invariant circles, and the line L_3 is fitted by these points.

Local behavior of the three-degree-of-freedom vibratory system with symmetrical stops, near the point of double Neimark–Sacker bifurcation, is obtained by numerical simulation. The partial bifurcation set near the critical value is plotted in Fig. 13, in which 1-1-1 symmetrical motion is represented by (S), and the symbol "Hopf Bif" represents Hopf Bifurcation of fixed point of 1-1-1 symmetrical motion, i.e., Neimark–Sacker bifurcation. On the line L_1 of Fig. 13 subcritical Neimark–Sacker bifurcation associated with period-one double-impact symmetrical motion occurs, and on the line L_2 supcritical Neimark–Sacker bifurcation of the motion occurs. On the line L_3 torus bifurcation occurs, which means that the quasi-periodic attractor, represented by the close circle, becomes quasi-attracting so that a new "tire-like" quasi-periodic attractor is possibly born near the line L_3. As γ is fixed, the 1-1-1 symmetrical motion will undergo supcritical Neimark–Sacker bifurcation, with decrease in the forcing frequency ω, so that the quasi-periodic impact orbit is generated, which is represented by an attracting and closed invariant circle in projected Poincaré section. With further decrease in the forcing frequency ω, instability of the closed circle occurs so that a new quasi-periodic impact motion is possibly born near the value of torus bifurcation, which is represented by "tire-like" quasi-periodic attractor in the projected Poincaré section. Whereas the 1-1-1 symmetrical motion undergoes also subcritical Neimark–Sacker bifurcation with increase in the forcing frequency ω. Dynamical behavior of the system, near the point of double Neimark–Sacker bifurcation, are further illustrated by bifurcation diagrams, phase plane portrait, time trajectory and projected Poincaré sections plotted in Figs. 14–16.

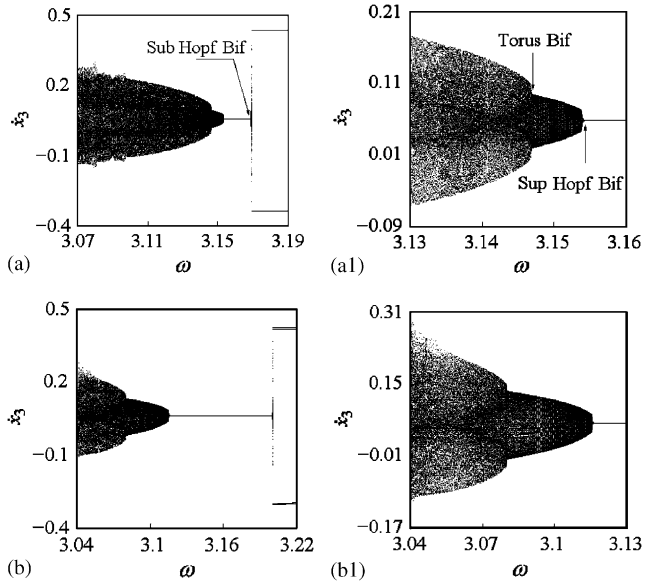

Fig. 14. Bifurcation diagrams near the point of double Neimark–Sacker bifurcation. (a) $\gamma = 0.061$, $\omega \in [3.07, 3.19]$ (a1) $\gamma = 0.061$, $\omega \in [3.13, 3.16]$, (b) $\gamma = 0.065$, $\omega \in [3.04, 3.22]$ (b1) $\gamma = 0.065$, $\omega \in [3.04, 3.13]$.

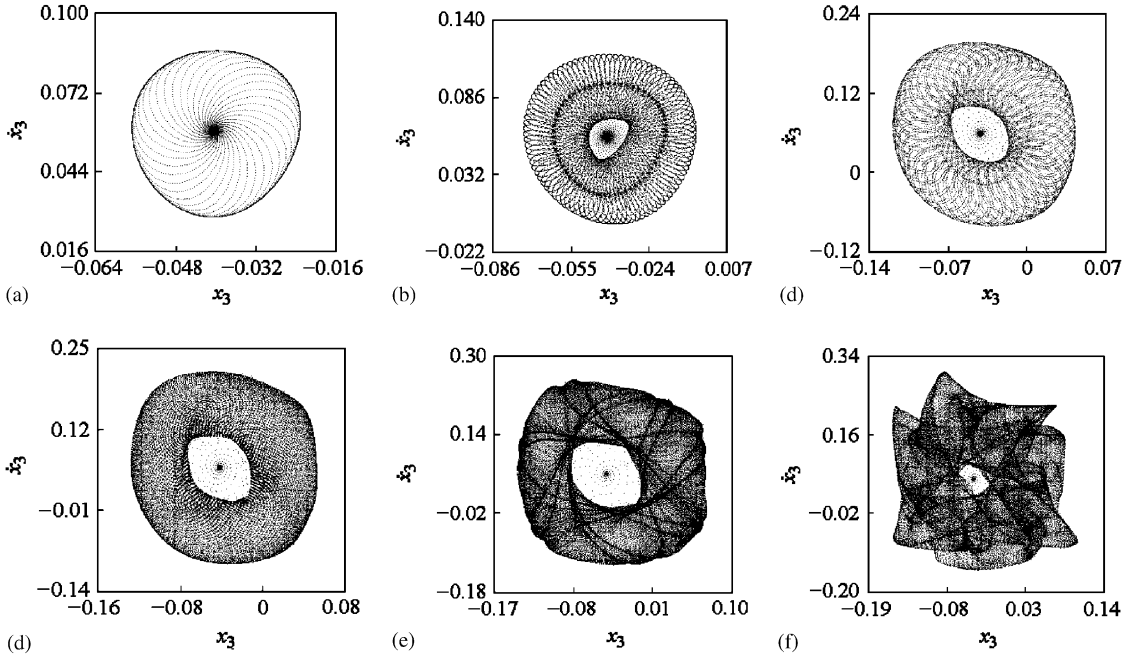

Fig. 15. Projected Poincaré sections: (a) transient points as well as the attracting invariant circle associated with 1-1-1 symmetrical motion, starting from the initial condition near the fixed point of 1-1-1 symmetrical motion, $\omega = 3.15$, $\gamma = 0.061$; (b) "tire-like" quasi-periodic attractor, $\omega = 3.146$, $\gamma = 0.061$; (c) "tire-like" quasi-periodic attractor, $\omega = 3.12$, $\gamma = 0.061$; (d) "tire-like" attractor, $\omega = 3.11$, $\gamma = 0.061$; (e) "tire-like" tori doubling, $\omega = 3.086$, $\gamma = 0.061$; (f) chaos, $\omega = 3.08$, $\gamma = 0.061$.

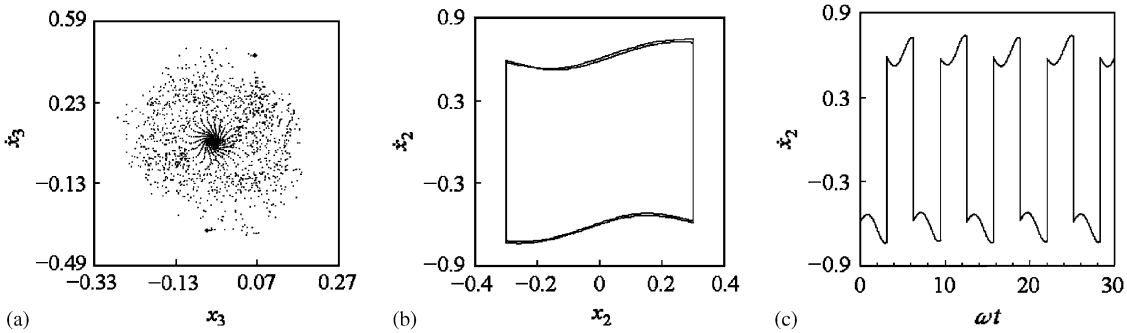

Fig. 16. Projected Poincaré section (a), phase plane portrait (b) and time trajectory (c): (a) transient points as well as the fixed points associated with 2-2-2 motion, starting from the initial condition near the fixed point (unstable focus) of 1-1-1 symmetrical motion, $\omega = 3.175$, $\gamma = 0.061$; (b) 2-2-2 motion, $\omega = 3.175$, $\gamma = 0.061$; (c) 2-2-2 motion, $\omega = 3.175$, $\gamma = 0.061$.

The fixed point associated with 1-1-1 symmetrical motion, with the corresponding parameter v, is taken as the initial map point in every numerical analysis. We choose $\gamma = 0.061$ and change the forcing frequency ω in numerical analyses. The results from simulation show that the system exhibits stable 1-1-1 symmetrical motion in the forcing frequency range $\omega \in (3.154923, 3.168377)$.

Instability of 1-1-1 symmetrical motion occurs, and supercritical Neimark–Sacker bifurcation associtated with the motion is generated as ω is decreased gradually and passes through $\omega_{c1} = 3.154923$. The system begins to exhibit the quasi-periodic impact motion, which is represented by an attracting and closed invariant circle in projected Poincaré section; see Fig. 15(a). With decrease in the forcing frequency ω, instability of the closed circle occurs so that a new quasi-periodic impact motion is born near the value of torus bifurcation,

which is represented by "tire-like" quasi-periodic attractor in the projected Poincaré section; see Figs. 15(b) and (c). As the forcing frequency is further decreased, the system finally falls into apparent chaotic motion via "tire-like" tori doubling, see Figs. 15(e) and (f).

Increase in the forcing frequency leads to instability and subcritical Neimark–Sacker bifurcation of 1-1-1 symmetrical motion. At the critical value $\omega_{c2} = 3.168377$, the eigenvalues of Jacobian matrix $Df(\omega, X^*)$ are given as follows:

$$\lambda_{1,2}(\omega_{c2}) = -0.5429462 \pm 0.8336944i,$$

$$|\lambda_{1,2}(\omega_{c2})| = 0.9949055,$$

$$\lambda_{3,4}(\omega_{c2}) = -0.9889936 \pm 0.1479582i,$$

$$|\lambda_{3,4}(\omega_{c2})| = 1.0000001,$$

$$\lambda_{5,6}(\omega_{c2}) = -0.2560790 \pm 0.1331653i, \quad |\lambda_{5,6}(\omega_{c2})| = 0.2886338.$$

It is found, by numerical simulation, that subcritical Neimark–Sacker bifurcation of 1-1-1 symmetrical motion occurs for $\omega > 3.168377$, and the fixed point associated with 1-1-1 symmetrical motion varies from stable focus to unstable focus. Fig. 16(a) shows transient points as well as the fixed points associated with 2-2-2 motion, starting from the initial condition near the fixed point (unstable focus) of 1-1-1 symmetrical motion for $\omega = 3.175$. Fig. 16(b) and (c) shows phase plane portrait and time trajectory of 2-2-2 motion for $\omega = 3.175$, respectively.

We have found, by analytical analyses and numerical simulation, that the vibro-impact systems with more than two degrees of freedom more easily work near the point of codimension two bifurcation than two-degree-of-freedom vibro-impact systems do. The increase in the number of equations correspondingly increases the number of eigenvalues of maps, which makes it possible that more eigenvalues lie near the unit circle of complex plane. An example is given in the following test. The system with parameters (2): $m_2 = 3$, $m_3 = 1.2$, $k_2 = 1.2$, $k_3 = 1.5$, $f_{10} = 0$, $f_{20} = 1$, $f_{30} = 0$, $\delta = 0.3$, $R = 0.7$ and $\gamma = 0.05$ has been chosen for analysis. The original purpose of the example is only used for analyzing dynamical behavior of the system near the point of strong resonance(1:2, $\lambda_1 = \bar{\lambda}_2$, $\lambda_{1,2}^2 = 1$). However, we find that the system exhibits quasi-periodic impact motion represented by "tire-like" quasi-periodic attractor. Its dynamical behavior is similar to that near the point of double Neimark–Sacker bifurcation. Here, we consider the case of $v \in \boldsymbol{R}^1$ and take only the forcing frequency ω as the control parameter. As ω passes through $\omega_c = 2.178259$ in a decreasing way, a complex conjugate pair of eigenvalues of $Df(\omega, 0)$ escape the unit circle from the points near the point $(-1, 0)$, the remainder of the spectrum of $Df(\omega, 0)$ stay still inside the unit circle, Neimark–Sacker or subharmonic bifurcation associated with 1:2 strong resonance case ($\lambda_{1,2}^2(\omega_c) = 1$) may occur. At the critical value $\omega_c = 2.178259$, the eigenvalues of Jacobian matrix $Df(\omega, 0)$ are given as follows:

$$\lambda_{1,2}(\omega_c) = -0.9999983 \pm 0.00019224i, \quad |\lambda_{1,2}(\omega_c)| = 1.0000001,$$

$$\lambda_{3,4}(\omega_c) = -0.5068009 \pm 0.7751092i, \quad |\lambda_{3,4}(\omega_c)| = 0.9260893,$$

$$\lambda_{5,6}(\omega_c) = -0.22575470 \pm 0.19433770i, \quad |\lambda_{5,6}(\omega_c)| = 0.2978797.$$

The numerical results show that the system exhibits stable 1-1-1 symmetrical motion for $\omega > 2.178259$. As ω passes through $\omega_c = 2.178259$ decreasingly, instability of the symmetrical double-impact periodic motion occurs so that the quasi-periodic impact motion, represented by the attracting invariant circle, is born; see Fig. 17(a). Decrease in the forcing frequency ω leads to that the closed circle becomes quasi-attracting, and the "tire-like" quasi-periodic attractor is born, see Figs. 17(b) and (c). With further decrease in the forcing frequency ω, the "tire-like" attractor gradually expands as seen in Figs. 17 (d) and (e) and finally ruptures, and the system falls into apparent chaotic motion; see Fig. 17(f). Afterwards a quasi-periodic attractor, represented by four attracting invariant circles, is born by a degeneration of chaos; see Fig. 17(g). With continuous decrease in ω, the invariant circles become quasi-attracting, and the system falls into chaotic motion again via the quasi-attracting invariant circles as seen in Figs. 17(h) and (i). The reason why the system with parameters

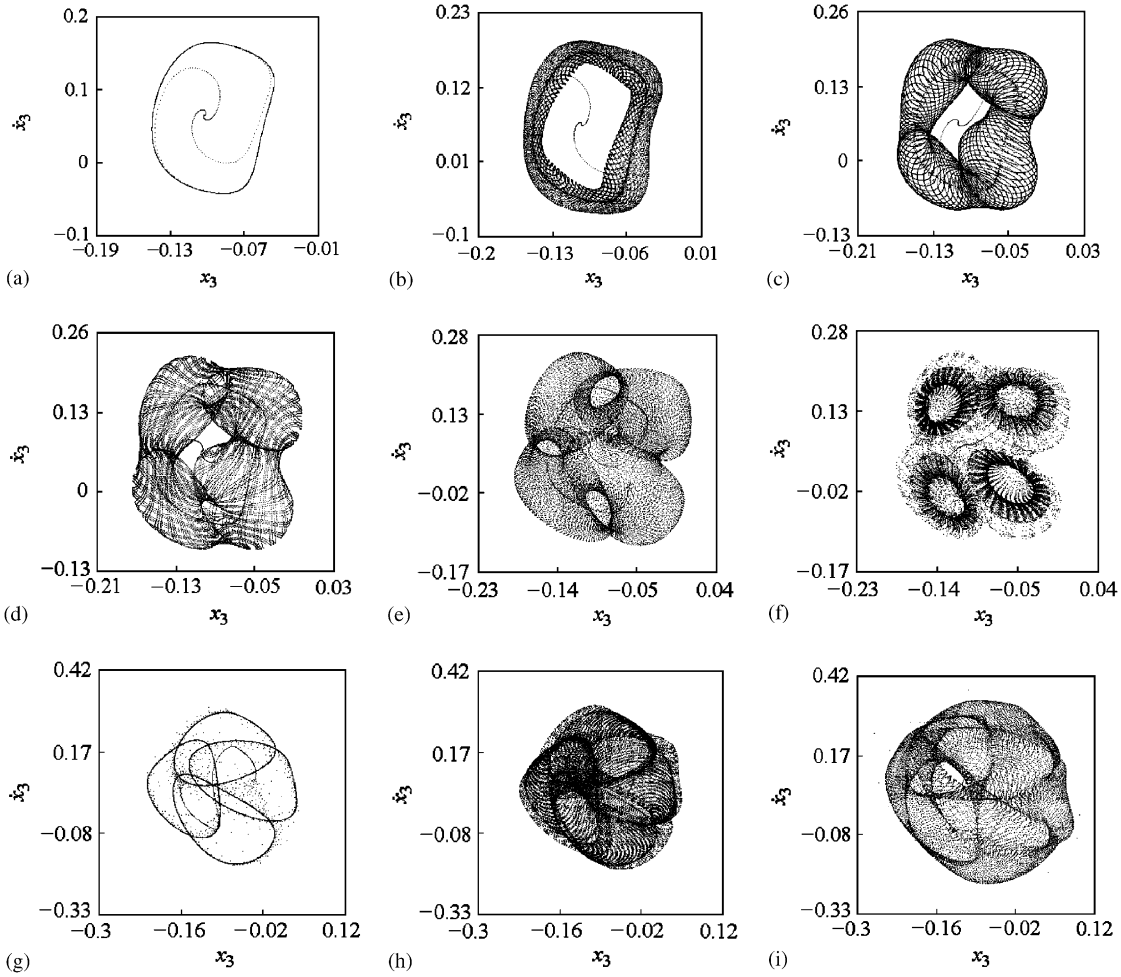

Fig. 17. Projected Poincaré sections: (a) transient points as well as the attracting invariant circle associated with 1-1-1 symmetrical motion, starting from the initial condition near the fixed point of 1-1-1 symmetrical motion, $\omega = 2.14$; (b) "tire-like" quasi-periodic attractor, $\omega = 2.135$; (c) "tire-like" quasi-periodic attractor, $\omega = 2.133$; (d) "tire-like" quasi-periodic attractor, $\omega = 2.132$; (e) "tire-like" attractor, $\omega = 2.13$; (f) chaos, $\omega = 2.124096$; (g) quasi-periodic attractor represented by four attracting invariant circles, $\omega = 2.1175$; (h) chaos, $\omega = 2.115$; (i) chaos, $\omega = 2.09$.

(2), in 1:2 strong resonance case, exhibits the "tire-like" quasi-periodic attractors is explained in the following test.

Let us continue to consider the system with parameters (2). Here, the forcing frequency ω and γ are taken as the control parameters, i.e. $v = (\gamma, \omega)^{\mathrm{T}}$. The eigenvalues of $Df(v, 0)$ are computed with $\omega \in [2.18, 2.3]$ and $\gamma \in [0.036, 0.05]$. The moduli of all eigenvalues of $Df(v, 0)$ are less than one for $v = (0.05,\ 2.18)^{\mathrm{T}}$. By gradually decreasing γ and increasing ω from the point $v = (0.05,\ 2.18)^{\mathrm{T}}$ to change the control parameter v, we can obtain two complex conjugate pairs of eigenvalues $\lambda_{1,2}(v_c) = -0.97662440 \pm 0.21495570i$ ($|\lambda_{1,2}(v_c)| = 1.00000000$), $\lambda_{3,4}(v_c) = -0.6300049 \pm 0.7765909i$ ($|\lambda_{3,4}(v_c)| = 0.9999998$) which are very close to the unit circle, and the other eigenvalues $\lambda_{5,6}(v_c) = -0.232266 \pm 0.2123674i$ ($|\lambda_{5,6}(v_c)| = 0.314718$) still stay inside the unit circle as v equals $v_c = (0.0399601,\ 2.258997)^{\mathrm{T}}$. The eigenvalues $\lambda_{1,2}(v)$ and $\lambda_{3,4}(v)$ have escaped the unit circle as ω and γ pass through $\omega = 2.258999$ (increasingly) and $\gamma = 0.03996$ (decreasingly). The eigenvalues $\lambda_{1,2}(v)$ and $\lambda_{3,4}(v)$ almost escape the unit circle simultaneously, so $v_c = (0.0399601,\ 2.258997)^{\mathrm{T}}$ is approximately taken as the value of double Neimark–Sacker bifurcation.

The partial bifurcation set near the critical value is plotted in Fig. 18. On the line L_1 of Fig. 18 subcritical Neimark–Sacker bifurcation of period-one double-impact symmetrical motion occurs, and on the line L_2

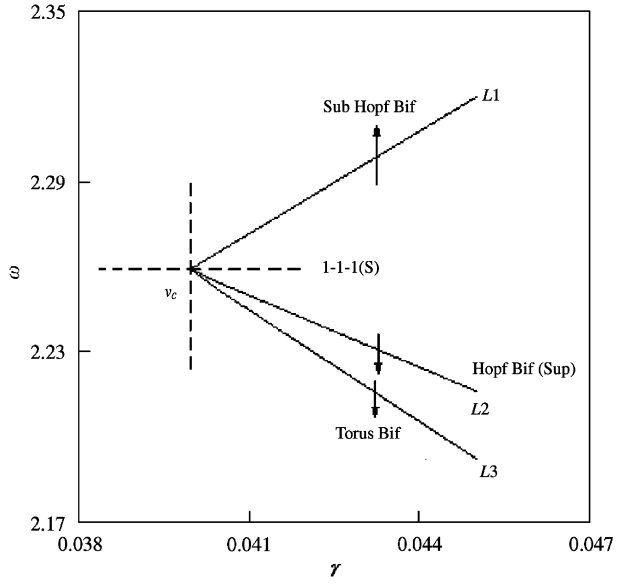

Fig. 18. The partial bifurcation set near the point of double Neimark–Sacker bifurcation.

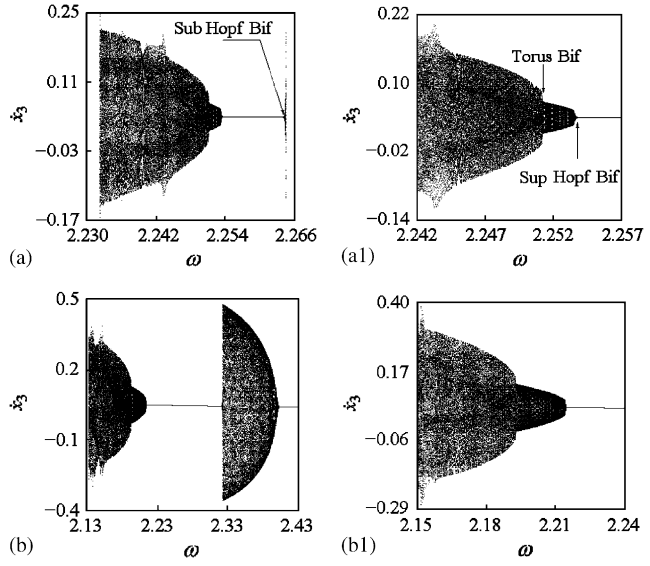

Fig. 19. Bifurcation diagrams near the point of double Neimark–Sacker bifurcation. (a) $\gamma = 0.0405$, $\omega \in [2.23, 2.26]$ (a1) $\gamma = 0.0405$, $\omega \in [2.242, 2.257]$, (b) $\gamma = 0.045$, $\omega \in [2.13, 2.43]$ (b1) $\gamma = 0.045$, $\omega \in [2.15, 2.24]$.

supcritical Neimark–Sacker bifurcation of the motion occurs. On the line L_3 torus bifurcation occurs, which means that the quasi-periodic attractor, represented by the close circle in Poincaré section, becomes quasi-attracting so that a new "tire-like" quasi-periodic attractor is born near the line L_3.

Some bifurcation diagrams and projected Poincaré sections are shown in Figs. 19 and 20, which illustrate dynamical behavior of the system with parameters (2) near the point of double Neimark–Sacker bifurcation.

According to the analysis above-mentioned, we can find that the point $v = (0.05, 2.178259)^{\mathrm{T}}$ of 1:2 strong resonance lies just near the point $v = (0.0399601, 2.258997)^{\mathrm{T}}$ of double Neimark–Sacker bifurcation. So the system with parameters (2), in 1:2 strong resonance case, also exhibits the quasi-periodic impact motion

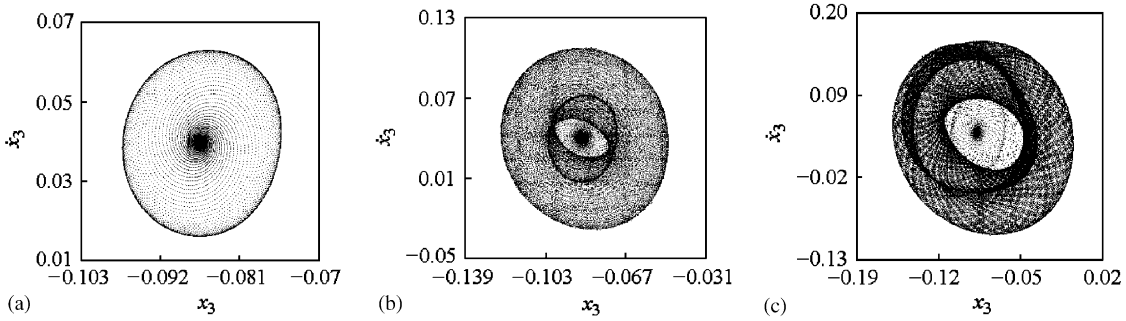

Fig. 20. Projected Poincaré sections: (a) the attracting invariant circle associated with 1-1-1 symmetrical motion; $\omega = 2.252$; (b) "tire-like" attractor, $\omega = 2.25$; (c) "tire-like" torus doubling, $\omega = 2.244$.

represented by "tire-like" quasi-periodic attractor. The quasi-periodic impact behavior is rich and complex. This means that two or more complex conjugate pairs of eigenvalues of maps, lying near the unit circle, possibly lead to the "tire-like" attractor.

By studying codimension two Neimark–Sacker bifurcations of vibro-impact system of Fig. 12, we can find that the system exhibit similar dynamical behavior near the points of codimension two Neimark–Sacker bifurcations. The analyses in the section show that near the point of double Neimark–Sacker bifurcation there exist period-one doubling-impact symmetrical motion, Neimark–Sacker bifurcation of the motion and torus bifurcation associated with the transition of the attracting invariant circle to "tire-like" attractor. The torus bifurcation leads to the quasi-attracting invariant circle and "tire-like" attractors. The quasi-attracting invariant circle is attracting for the map point inside the circle, and repelling for the map point on or outside it. The "tire-like" attractor is of quasi-periodic impact characteristics near the point of torus bifurcation. The dynamic behavior of the vibro-impact system shown in Figs. 13–16 (and Figs. 18–20), near the point of double Neimark–Sacker bifurcation, corresponds with the unfolding of case 6(a) of the normal form map which is shown in Figs. 8 and 10. Moreover, by numerical simulation we also observe the dynamic behavior of the vibro-impact system corresponding with the unfolding of the normal form map associated with cases 5, 6(b), 7(b) and 8. In the four cases, the dynamic behaviors of the vibro-impact system are simpler than those shown in Figs. 13 and 18, the system exhibits only the quasi-periodic attractor represented by an attracting and closed circle, and no stable "tire-like" quasi-periodic attractor occurs; one of two Neimark–Sacker bifurcations associated with 1-1-1 symmetrical motion is supercritical, and the other is subcritical.

7. Conclusions

An important application where the model studied here may be of use is in the dynamics of heat exchanger tubes in nuclear reactors [51]. Such tubes are designed to have clearances at support points to allow for thermal expansion. When fluid flows past these tubes vortex shedding occurs and the tubes are excited. The response of such systems is very complicated [51] and the wearing of these tubes is a major problem in the nuclear industry. Fluid flow past panels and beams can result in chaotic motions and thus bifurcation behavior and chaotic motions may provide an appropriate tool in the study of tube wear. The other important application where the model may also be of use is in the vibro-impact dynamics of wheelset and rail of high speed railway coaches [26]. At low speeds the coaches will undergo nonlinear oscillations and behave as a self-excited nonlinear system without impacts. As the speed of coaches is increased, the coaches exhibit hunting motion and the flange of wheelset eventually begins to hit the steel rail. Some researches into symmetrical double-impact periodic motion, stability, pitchfork bifurcation and routes to chaos were developed for the vibratory systems with symmetrical rigid stops in Refs. [3,16].

No Neimark–Sacker bifurcation of symmetrical double-impact periodic motion occurs in a single-degree-of-freedom system having symmetrically placed rigid stops and subjected to periodic excitation [3]. However,

in the paper Neimark–Sacker bifurcations of 1-1-1 symmetrical motions are shown to exist in the multidegree-of-freedom vibro-impact system with symmetrical rigid stops. As the forcing frequency is changed, the quasi-periodic impact motion may lead to chaos via torus bifurcation and "tire-like" tori doubling successively.

Double Neimark–Sacker bifurcation of the vibratory system with symmetrical rigid stops is analyzed in the paper. Local behavior of the system, near the point of double Neimark–Sacker bifurcation, is investigated by using qualitative analysis and numerical simulation. Near the value of double Neimark–Sacker bifurcation there exist period-one double-impact symmetrical motion and quasi-periodic impact motions. The quasi-periodic impact motions are represented by the closed circle and "tire-like" quasi-periodic attractor in projected Poincaré sections, respectively. Complex dynamic behavior near the points of codimension two bifurcations is observed by means of two examples in Section 6, which corresponds with the unfolding of the simplified map in case 6(a) shown in Figs. 8 and 10. One of two Neimark–Sacker bifurcations associated with 1-1-1 symmetrical motion is supercritical, and the other is subcritical; after the supercritical Neimark–Sacker bifurcation, torus bifurcation, associated with the transition of the attracting invariant circle to "tire-like" attractor, occurs with change of control parameters. Routes from "tire-like" quasi-periodic attractors to chaos are stated briefly. However, it should be noted that routes from "tire-like" quasi-periodic attractor to chaos have not been known well.

The strict condition of codimension two bifurcation is not easy to encounter in practical application of engineering. However, there exist the possibilities that actual nonlinear dynamical systems, with two varying parameters or more, work near the critical value of codimension two bifurcation due to change of parameters. The impact-forming machinery is a typical example [52]. Besides the forcing frequency ω, the value of gap varies also with different thickness of the formed workpieces. Another representative example is the inertial vibro-impact shaker, of which the distribution of masses is generally metabolic with the casts with different masses, and the forcing frequency is also important parameter changed [53]. The change of multiparameters possibly leads to the results that the vibro-impact systems work near the critical parametres of codimension two bifurcation. It is necessary to study the bifurcations caused by change of multiparameters to reveal dynamical behavior of nonlinear systems near the points of bifurcations.

Acknowledgement

The authors gratefully acknowledge the support by National Natural Science Foundation (10572055, 50475109), Natural Science Foundation of Gansu Province Government of China (ZS-011-A25-010-Z, ZS-031-A25-007-Z (key item)) and 'Qing Lan' Talent Engineering by Lanzhou Jiaotong University.

Appendix A

Let Ψ represent the canonical modal matrix of Eq. (2), ω_i $(i = 1, 2, \ldots, n)$ denote the eigenfrequiencies of the system, $\eta_i = \gamma\omega_i$, $\omega_{di} = \omega_i\sqrt{1-\eta_i^2}$. Using the formal coordinate and modal matrix approach, one can obtain the general solutions of Eq. (2):

$$x(t) = \Psi\xi(t), \tag{A.1}$$

$$\xi(t) = G(t)A_1 + H(t)B_1 + F_s\sin(\omega t+\tau) + F_c\cos(\omega t+\tau), \quad 0 \leqslant t \leqslant t_1, \tag{A.2}$$

$$\xi(t) = G(t-t_1)A_2 + H(t-t_1)B_2 + F_s\sin(\omega t+\tau) + F_c\cos(\omega t+\tau), \quad t_1 < t \leqslant t_1+t_2 \tag{A.3}$$

in which, it takes the time t_1 and t_2 for the mass M_k to move from the constraint A to $\bar{A}$ and from the constraint $\bar{A}$ to A, respectively; A_1, A_2, B_1 and B_2 are the constant matrixes of integration, $G(t) = \mathrm{diag}[e^{-\eta_i\omega_i t}\sin(\omega_{di}t)]$, $H(t) = \mathrm{diag}[e^{-\eta_i\omega_i t}\cos(\omega_{di}t)]$, $i = 1, 2, \ldots, n$ (The symbol "diag[ ]" is used to denote the diagonal matrix); $F_s = (f_{s1}, f_{s2}, \ldots, f_{sn})^{\mathrm{T}}$ and $F_c = (f_{c1}, f_{c2}, \ldots, f_{cn})^{\mathrm{T}}$ are the amplitude constant vectors.

The determination of the period-one double-impact symmetrical motion is based on the fact that they satisfy the following set of periodicity and matching conditions:

$$\begin{bmatrix} x(0) \\ \dot{x}(0) \end{bmatrix} = -\begin{bmatrix} x(\pi/\omega)_+ \\ \dot{x}(\pi/\omega)_+ \end{bmatrix} = D\begin{bmatrix} x(2\pi/\omega) \\ \dot{x}(2\pi/\omega) \end{bmatrix} = \begin{bmatrix} x_0 \\ \dot{x}_0 \end{bmatrix}, \quad \begin{bmatrix} x(\pi/\omega)_- \\ \dot{x}(\pi/\omega)_- \end{bmatrix} = -\begin{bmatrix} x(2\pi/\omega) \\ \dot{x}(2\pi/\omega) \end{bmatrix}, \tag{A.4}$$

where $D = \mathrm{diag}[d_i]$, $(d_i = 1,\ i = 1, 2, \ldots, k, \ldots, n+k-1, n+k+1, \ldots, 2n;\ d_{n+k} = -R)$, $x_0 = (x_{10}, x_{20}, \ldots, x_{(k-1)0}, \delta, x_{(k+1)0}, \ldots, x_{n0})^{\mathrm{T}}$, $\dot{x}_0 = (\dot{x}_{10}, \dot{x}_{20}, \ldots, \dot{x}_{(k-1)0}, \dot{x}_{k+}, \dot{x}_{(k+1)0}, \ldots, \dot{x}_{n0})^{\mathrm{T}}$. Letting $\bar{t}_1 = \pi/\omega$, $\bar{t}_2 = \pi/\omega$, $\tilde{g}_i(t) = \mathrm{e}^{\eta_i\omega_i t}\sin(\omega_{di}t)$, $\tilde{h}_i(t) = \mathrm{e}^{\eta_i\omega_i t}\cos(\omega_{di}t)$, $g_i(t) = \mathrm{e}^{-\eta_i\omega_i t}\sin(\omega_{di}t)$, $h_i(t) = \mathrm{e}^{-\eta_i\omega_i t}\cos(\omega_{di}t)$, one can express 1-1-1 symmetrical response by

$$x(t) = \Psi P_{11}(t)\Psi^{-1}x(0) + \Psi P_{12}(t)\Psi^{-1}\dot{x}(0) + P_{s1}(t)\sin\tau + P_{c1}(t)\cos\tau, \quad 0 \leqslant t \leqslant \bar{t}_1, \tag{A.5}$$

$$x(t) = \Psi P_{21}(t)\Psi^{-1}x(2\pi/\omega) + \Psi P_{22}(t)\Psi^{-1}\dot{x}(2\pi/\omega) + P_{s2}(t)\sin\tau + P_{c2}(t)\cos\tau, \quad \bar{t}_1 < t \leqslant \bar{t}_1 + \bar{t}_2 \tag{A.6}$$

in which, $P_{11}(t) = \mathrm{diag}[g_i(t)\eta_i\omega_i/\omega_{di} + h_i(t)]$, $P_{12}(t) = \mathrm{diag}[g_i(t)/\omega_{di}]$,

$$P_{21}(t) = \mathrm{diag}[\tilde{h}_i(2\pi/\omega)(g_i(t)\eta_i\omega_i/\omega_{di} + h_i(t)) - \tilde{g}_i(2\pi/\omega)(h_i(t)\eta_i\omega_i/\omega_{di} - g_i(t))],$$

$$P_{22}(t) = \mathrm{diag}[(g_i(t)\tilde{h}_i(2\pi/\omega) - \tilde{g}_i(2\pi/\omega)h_i(t))/\omega_{di}],$$

$$P_{si}(t) = \Psi(F_s\cos\omega t - F_c\sin\omega t + P_{i2}(t)\,\omega F_c - P_{i1}(t)F_s),$$

$$P_{ci}(t) = \Psi(F_s\sin\omega t + P_c\cos\omega t - P_{i2}(t)\omega F_s - P_{i1}(t)F_c)$$

Letting $\Phi = \mathrm{diag}[\Psi, \Psi]$, and

$$P_i(t) = \begin{bmatrix} P_{i1}(t) & P_{i2}(t) \\ \dot{P}_{i1}(t) & \dot{P}_{i2}(t) \end{bmatrix}, \quad Q_i(t) = \begin{bmatrix} P_{si}(t) & P_{ci}(t) \\ \dot{P}_{si}(t) & \dot{P}_{ci}(t) \end{bmatrix},$$

the response of 1-1-1 symmetrical orbit is given by

$$\begin{bmatrix} x(t) \\ \dot{x}(t) \end{bmatrix} = \Phi P_1(t)\Phi^{-1}\begin{bmatrix} x(0) \\ \dot{x}(0) \end{bmatrix} + Q_1(t)\begin{bmatrix} S_\tau \\ C_\tau \end{bmatrix}, \quad 0 \leqslant t \leqslant \bar{t}_{1-}, \tag{A.7}$$

$$\begin{bmatrix} x(t) \\ \dot{x}(t) \end{bmatrix} = \Phi P_2(t)\Phi^{-1}D^{-1}\begin{bmatrix} x(0) \\ \dot{x}(0) \end{bmatrix} + Q_2(t)\begin{bmatrix} S_\tau \\ C_\tau \end{bmatrix}, \quad \bar{t}_{1+} \leqslant t \leqslant \bar{t}_1 + \bar{t}_2, \tag{A.8}$$

where $S_\tau = \sin\tau$, $C_\tau = \cos\tau$.

Substituting formula (A.4) and inserting $t = 2\pi/\omega$ to formula (A.8), one obtains the following equation:

$$\begin{bmatrix} x(0) \\ \dot{x}(0) \end{bmatrix} = D[L - \Phi P_2(2\pi/\omega)\Phi^{-1}]^{-1}Q_2(2\pi/\omega)\begin{bmatrix} S_\tau \\ C_\tau \end{bmatrix}, \tag{A.9}$$

where L is a unit matrix of degree $2n \times 2n$. Let $E = D[L - \Phi P_2(2\pi/\omega)\Phi^{-1}]^{-1}Q_2(2\pi/\omega)$, then $E = [e_{ij}]$ is a matrix of degree $2n \times 2$.

According to the periodicity and matching conditions (A.4), one obtains the kth component $x_k(0)$ from formula (A.9), which is now

$$x_k(0) = \delta = e_{k1}\sin\tau_0 + e_{k2}\cos\tau_0. \tag{A.10}$$

Solving formula (A.10) and substituting τ_0 into the solutions (A.7) and (A.8), we obtain the analytical expression for period-one double-impact symmetrical orbit.

If 1-1-1 symmetrical motion is disturbed at the instant of impact by the difference ΔX, then one can express the differences $\Delta X'$ at the instant of the next impact. Between two consecutive impacts occurring at the stop A,

the disturbed solutions of 1-1-1 symmetrical motion are written in the form

$$\begin{bmatrix}\tilde{x}(t)\\ \dot{\tilde{x}}(t)\end{bmatrix} = \Phi\tilde{E}(t)\begin{bmatrix}\tilde{A}_1\\ \tilde{B}_1\end{bmatrix} + \Phi U\tilde{Q}\begin{bmatrix}\tilde{S}_t\\ \tilde{C}_t\end{bmatrix}, \quad 0 \leqslant t \leqslant \tilde{t}_{1-}, \tag{A.11}$$

$$\begin{bmatrix}\tilde{x}(t)\\ \dot{\tilde{x}}(t)\end{bmatrix} = \Phi\tilde{E}(t-\tilde{t}_1)\begin{bmatrix}\tilde{A}_2\\ \tilde{B}_2\end{bmatrix} + \Phi U\tilde{Q}\begin{bmatrix}\tilde{S}_t\\ \tilde{C}_t\end{bmatrix}, \quad \tilde{t}_{1+} \leqslant t \leqslant t_e, \tag{A.12}$$

where $\tilde{S}_t = \sin(\omega t + \tau_0 + \Delta\tau)$, $\tilde{C}_t = \cos(\omega t + \tau_0 + \Delta\tau)$, $\tilde{t}_1 = \pi/\omega + \Delta t_1$, $\tilde{t}_2 = \pi/\omega + \Delta t_2$, $t_e = \tilde{t}_1 + \tilde{t}_2$,

$$\tilde{E}(t) = \begin{bmatrix}G(t) & H(t)\\ \dot{G}(t) & \dot{H}(t)\end{bmatrix}, \quad \tilde{Q} = \begin{bmatrix}F_s & F_c\\ -F_c & F_s\end{bmatrix}, \quad U = \begin{bmatrix}I & \\ & \omega I\end{bmatrix},$$

I is a unit matrix of degree $n \times n$.

The dimensionless time is set to zero directly after an impact occurring at the constraint A, it becomes $(2\pi + \Delta\theta)/\omega$ just before the next impact occurring at the same stop, and $\Delta\theta = \omega(\Delta t_1 + \Delta t_2)$. Letting $t_e = (2\pi + \Delta\theta)/\omega$, the impact boundary conditions of the disturbed motion are expressed by

$$\begin{bmatrix}\tilde{x}(0)\\ \dot{\tilde{x}}(0)\end{bmatrix} = \begin{bmatrix}x_0 + \Delta x\\ \dot{x}_0 + \Delta\dot{x}\end{bmatrix}, \quad \begin{bmatrix}\tilde{x}(\tilde{t}_{1+})\\ \dot{\tilde{x}}(\tilde{t}_{1+})\end{bmatrix} = \begin{bmatrix}-x_0 + \Delta x''\\ -\dot{x}_0 + \Delta\dot{x}''\end{bmatrix}, \quad \begin{bmatrix}\tilde{x}(\tilde{t}_{1+})\\ \dot{\tilde{x}}(\tilde{t}_{1+})\end{bmatrix} = D\begin{bmatrix}\tilde{x}(\tilde{t}_{1-})\\ \dot{\tilde{x}}(\tilde{t}_{1-})\end{bmatrix}, \quad D\begin{bmatrix}\tilde{x}(t_e)\\ \dot{\tilde{x}}(t_e)\end{bmatrix} = \begin{bmatrix}x_0 + \Delta x'\\ \dot{x}_0 + \Delta\dot{x}'\end{bmatrix}. \tag{A.13}$$

Inserting the boundary conditions (A.13) into the disturbed solutions (A.11) and (A.12) for $t = 0$ and $t = \tilde{t}_{1+}$, respectively, one can solve

$$\begin{bmatrix}\tilde{A}_1\\ \tilde{B}_1\end{bmatrix} = [\Phi\tilde{E}(0)]^{-1}\begin{bmatrix}x_0 + \Delta x\\ \dot{x}_0 + \Delta\dot{x}\end{bmatrix} - [\Phi\tilde{E}(0)]^{-1}\Phi U\tilde{Q}\begin{bmatrix}\tilde{S}_{\Delta\tau}\\ \tilde{C}_{\Delta\tau}\end{bmatrix}, \tag{A.14}$$

$$\begin{bmatrix}\tilde{A}_2\\ \tilde{B}_2\end{bmatrix} = \left[\Phi\tilde{E}(0)\right]^{-1}\begin{bmatrix}-x_0 + \Delta x''\\ -\dot{x}_0 + \Delta\dot{x}''\end{bmatrix} - \left[\Phi\tilde{E}(0)\right]^{-1}\Phi U\tilde{Q}\begin{bmatrix}\tilde{S}_{\tilde{t}_1}\\ \tilde{C}_{\tilde{t}_1}\end{bmatrix} \tag{A.15}$$

in which, $\tilde{S}_{\Delta\tau} = \sin(\tau_0 + \Delta\tau)$, $\tilde{C}_{\Delta\tau} = \cos(\tau_0 + \Delta\tau)$, $\tilde{S}_{\tilde{t}_1} = \sin(\omega\tilde{t}_1 + \tau_0 + \Delta\tau)$, $\tilde{C}_{\tilde{t}_1} = \cos(\omega\tilde{t}_1 + \tau_0 + \Delta\tau)$.

Substituting formula (A.15) into the disturbed solution (A.12), and then taking $t = \tilde{t}_1$, one obtains, from the kth term of the disturbed solution (A.11), the following formula:

$$\begin{aligned}\tilde{x}_k(\tilde{t}_1) = {} & \psi_k(G(\pi/\omega + \Delta t_1)\tilde{A}_1 + H(\pi/\omega + \Delta t_1)\tilde{B}_1 - F_s\sin(\omega\Delta t_1 + \tau_0 + \Delta\tau)\\ & - F_c\cos(\omega\Delta t_1 + \tau_0 + \Delta\tau) = -\delta,\end{aligned} \tag{A.16}$$

where ψ_k is the kth row of the matrix Ψ.

Letting $\Delta X = (\Delta x_1, \Delta x_2, \ldots, \Delta x_{k-1}, \Delta\tau, \Delta x_{k+1}, \ldots, \Delta x_n, \Delta\dot{x}_1, \Delta\dot{x}_2, \ldots, \Delta\dot{x}_{k-1}, \Delta\dot{x}_{k+}, \Delta\dot{x}_{k+1}, \ldots, \Delta\dot{x}_n)^{\mathrm{T}} = (\Delta\tilde{y}_1, \Delta\tilde{y}_2, \ldots, \Delta\tilde{y}_{2n})^{\mathrm{T}}$, one can define the function

$$h(\Delta X, \Delta t_1) = \tilde{x}_k(\pi/\omega + \Delta t_1) + \delta = 0. \tag{A.17}$$

Supposing $(\partial h/\partial\Delta t_1)\big|_{\underbrace{(0,0,\cdots,0)}_{2n+1}} \neq 0$, using the implicit function theorem and solving Eq. (A.17) for Δt_1, one obtains

$$\Delta t_1 = (\Delta x_1, \Delta x_2, \ldots, \Delta x_{k-1}, \Delta\tau, \Delta x_{k+1}, \ldots, \Delta x_n, \Delta\dot{x}_1, \Delta\dot{x}_2, \ldots, \Delta\dot{x}_{k-1}, \Delta\dot{x}_{k+}, \Delta\dot{x}_{k+1}, \ldots, \Delta\dot{x}_n), \tag{A.18}$$

The partial derivative of Δt_1 with respect to ΔX can be expressed by

$$\frac{\partial\Delta t_1}{\partial\Delta\tilde{y}_i} = -\frac{\partial h}{\partial\Delta\tilde{y}_i}\Big/\left(\frac{\partial h}{\partial\Delta t_1}\right), \quad i = 1, 2, 3, \ldots, 2n. \tag{A.19}$$

Substituting the boundary conditions (A.13) into the disturbed solution (A.12) for $t = t_e$, one can obtain

$$\tilde{Y}_0 = \begin{bmatrix} x_0 + \Delta x' \\ \dot{x}_0 + \Delta \dot{x}' \end{bmatrix} = D\Phi\tilde{E}(\pi/\omega + \Delta t_2)\begin{bmatrix} \tilde{A}_2 \\ \tilde{B}_2 \end{bmatrix} + D\Phi U\tilde{Q}\begin{bmatrix} \tilde{S}_{\Delta t} \\ \tilde{C}_{\Delta t} \end{bmatrix}. \tag{A.20}$$

where $\tilde{S}_{\Delta t} = \sin(\omega\Delta t_1 + \omega\Delta t_2 + \tau_0 + \Delta\tau)$, $\tilde{C}_{\Delta t} = \cos(\omega\Delta t_1 + \omega\Delta t_2 + \tau_0 + \Delta\tau)$.

Taking the kth term of the state vector $\tilde{Y}_0$, one can define the function

$$\begin{aligned} &g(\Delta x_1, \Delta x_2, \ldots, \Delta x_{k-1}, \Delta\tau, \Delta x_{k+1}, \ldots, \Delta x_n, \Delta\dot{x}_1, \Delta\dot{x}_2, \ldots, \Delta\dot{x}_{k-1}, \\ &\quad \Delta\dot{x}_{k+}, \Delta\dot{x}_{k+1}, \ldots, \Delta\dot{x}_n, \Delta t_1, \Delta t_2) = \tilde{x}_k(t_e) - \delta = 0 \end{aligned} \tag{A.21}$$

Supposing $(\partial g/\partial\Delta t_2)|_{\underbrace{(0,0,\ldots,0)}_{2n+1}} \neq 0$, using the implicit function theorem and solving Eq. (A.21) for Δt_2, one obtains

$$\begin{aligned} \Delta t_2 = \Delta t_2(&\Delta x_1, \Delta x_2, \ldots, \Delta x_{k-1}, \Delta\tau, \Delta x_{k+1}, \ldots, \Delta x_n, \Delta\dot{x}_1, \\ &\Delta\dot{x}_2, \ldots, \Delta\dot{x}_{k-1}, \Delta\dot{x}_{k+}, \Delta\dot{x}_{k+1}, \ldots, \Delta\dot{x}_n, \Delta t_1). \end{aligned} \tag{A.22}$$

The partial derivative of Δt_2 with to ΔX can be expressed by

$$\frac{\partial\Delta t_2}{\partial\Delta\tilde{y}_i} = -\left(\frac{\partial g}{\partial\Delta\tilde{y}_i} + \frac{\partial g}{\partial\Delta t_1}\cdot\frac{\partial\Delta t_1}{\partial\Delta\tilde{y}_i}\right)\Big/\left(\frac{\partial g}{\partial\Delta t_2}\right), \quad i = 1, 2, \ldots, 2n. \tag{A.23}$$

Inserting Δt_1 and Δt_2 into the state vector (A.20), one gets finally the disturbed map of period-one double-impact symmetrical motion

$$X' = \tilde{f}(v, X) = D_1\tilde{Y}_0 + D_2 \tag{A.24}$$

in which, $D_1 = \mathrm{diag}[d_i^{(1)}]$, $d_i^{(1)} = 1, i = 1, \ldots, k-1, k+1, \cdots, 2n$, $d_k^{(1)} = 0$; $D_2 = \mathrm{diag}[d_i^{(2)}]$, $d_i^{(2)} = 0, i = 1, \ldots, k-1, k+1, \ldots, 2n$, $d_k^{(2)} = \tau'$, $\tau' = \tau_0 + \omega\Delta t_1 + \omega\Delta t_2$.

References

[1] P.J. Holmes, The dynamics of repeated impacts with a sinusoidally vibrating table, *Journal of Sound and Vibration* 84 (2) (1982) 173–189.

[2] S.W. Shaw, P.J. Holmes, A periodically forced piecewise linear oscillator, *Journal of Sound and Vibration* 90 (1) (1983) 129–155.

[3] S.W. Shaw, The dynamics of a harmonically excited system having rigid amplitude constraints: part 1, part 2, *Journal of Applied Mechanics* 52 (1985) 453–464.

[4] G.S. Whiston, Global dynamics of vibro-impacting linear oscillator, *Journal of Sound and Vibration* 118 (3) (1987) 395–429.

[5] C.S. Yim, H. Lin, Nonlinear impact and chaotic response of slender rocking objects, *Journal of Engineering. Mechanics* 117 (9) (1991) 2079–2100.

[6] S.L.T. de Souza, I.L. Caldas, Calculation of Lyapunov exponents in systems with impacts, *Chaos, Solitons and Fractals* 19 (3) (2004) 569–579.

[7] J.O. Aidanpää, B.R. Gupta, Periodic and chaotic behaviour of a threshold- limited two-degree-of-freedom system, *Journal of Sound and Vibration* 165 (2) (1993) 305–327.

[8] D.J. Wagg, Rising phenomena and the multi-sliding bifurcation in a two-degree of freedom impact oscillator, *Chaos, Solitons and Fractals* 22 (3) (2004) 541–548.

[9] K.M. Cone, R.I. Zadoks, An numerical study of an impact oscillator with the addition of dry friction, *Journal of Sound and Vibration* 188 (5) (1995) 659–683.

[10] D.P. Jin, H.Y. Hu, Periodic vibro-impacts and their stability of a dual component system, *Acta Mechanism Sinica* 13 (4) (1997) 366–376.

[11] A.B. Nordmark, Non-periodic motion caused by grazing incidence in an impact oscillator, *Journal of Sound and Vibration* 145 (2) (1991) 279–297.

[12] G.S. Whiston, Singularities in virbo-impact dynamics, *Journal of Sound and Vibration* 152 (3) (1992) 427–460.

[13] S. Foale, S.R. Bishop, Dynamical complexities of forced impacting systems, *Philosophical Transactions of the Royal Society of London* 338 (A) (1992) 547–556.

[14] A.P. Ivanov, Bifurcation in impact systems, *Chaos, Solitons and Fractal* 7 (10) (1996) 1615–1634.

[15] F. Peterka, Bifurcation and transition phenomena in an impact oscillator, *Chaos, Solitons and Fractals* 7 (10) (1996) 1635–1647.

[16] F. Peterka, J. Vacik, Transition to chaotic motion in mechanical systems with impacts, *Journal of Sound and Vibration* 154 (1) (1992) 95–115.

[17] C. Budd, F. Dux, A. Cliffe, The effect of frequency and clearance variations on single-degree- of-freedom impact oscillators, *Journal of Sound and Vibration* 184 (3) (1995) 475–502.
[18] M.I. Feigin, The increasingly complex structure of the bifurcation tree of a piecewise-smooth system, *Journal of Applied Mathematics and Mechanics* 59 (6) (1995) 853–863.
[19] D. Bernardo, M.I. Feigin, S.J. Hogan, M.E. Homer, Local analysis of C-bifurcations in N-dimensional piecewise-smooth dynamical systems, *Chaos, Solitons and Fractals* 10 (11) (1999) 1881–1908.
[20] D.T. Nguyen, S.T. Noah, C.F. Kettleborough, Impact behaviour of an oscillator with limiting stops, part I: a parametric study, *Journal of Sound and Vibration* 109 (2) (1986) 293–307.
[21] S. Natsiavas, Dynamics of multiple-degree-of-freedom oscillators with colliding components, *Journal of Sound and Vibration* 165 (3) (1993) 439–453.
[22] S. Chatterjee, A.K. Mallik, Bifurcations and chaos in autonomous self-excited oscillators with impact damping, *Journal of Sound and Vibration* 191 (4) (1996) 539–562.
[23] G.W. Luo, J.H. Xie, Hopf bifurcation of a two-degree-of-freedom vibro-impact system, *Journal of Sound and Vibration* 213 (3) (1998) 391–408.
[24] G.W. Luo, J.H. Xie, Stability of periodic motion, bifurcations and chaos of a two-degree-of-freedom vibratory system with symmetrical rigid stops, *Journal of Sound and Vibration* 273 (2) (2004) 543–568.
[25] H.Y. Hu, Controlling chaos of a periodically forced nonsmooth mechanical system, *Acta Mechanica Sinica* 11 (3) (1995) 251–258.
[26] J.P. Mejaard, A.D. De Pater, Railway vehicle systems dynamics and chaotic vibrations, *International Journal of Non-Linear Mechanics* 24 (1) (1989) 1–17.
[27] J. Zeng, S. Hu, Study on frictional impact and derailment for wheel and rail, *Journal of Vibration Engineering* 14 (1) (2001) 1–6.
[28] H. True, Dynamics of a rolling wheelset, *Applied Mechanics Reviews* 46 (7) (1993) 438–444.
[29] L.A. Wood, K.P. Byrne, Analysis of a random repeated impact process, *Journal of Sound and Vibration* 78 (3) (1981) 329–345.
[30] Z.L. Huang, Z.H. Liu, W.Q. Zhu, Stationary response of multi-degree-of-freedom vibro-impact systems under white noise excitations, *Journal of Sound and Vibration* 275 (1–2) (2004) 223–240.
[31] Z.Z. Shu, X.Z. Shen, Theoretical analysis of complete stability and automatic vibration isolation of impacting and vibrating systems with double masses, *Chinese Journal of Mechanical Engineering* 26 (3) (1990) 50–57.
[32] J.E. Kozol, R.M. Brach, Two-dimensional vibratory impact and chaos, *Journal of Sound and Vibration* 148 (2) (1991) 319–327.
[33] J.H. Xie, The mathematical model for the impact hammer and global bifurcations, *Acta Mechanica Sinica* 29 (4) (1997) 456–463.
[34] J.M.T. Thompson, Complex dynamics of compliant offshore structures, *Proceedings of the Royal Society of London A* 387 (1983) 407–427.
[35] C.K. Sung, W.S. Yu, Dynamics of harmonically excited impact damper: bifurcations and chaotic motion, *Journal of Sound and Vibration* 158 (2) (1992) 317–329.
[36] C.N. Bapat, C. Bapat, Impact-pair under periodic excitation, *Journal of Sound and Vibration* 120 (1) (1988) 53–61.
[37] P.R.S. Han, A.C.J. Luo, Chaotic motion of a horizontal impact pair, *Journal of Sound and Vibration* 181 (2) (1995) 231–250.
[38] M.S. Heiman, A.K. Bajaj, P.J. Sherman, Periodic motions and bifurcations in dynamics of an inclined impact pair, *Journal of Sound and Vibration* 124 (1) (1988) 55–78.
[39] C.N. Bapat, The general motion of an inclined impact damper with friction, *Journal of Sound and Vibration* 184 (3) (1995) 417–427.
[40] A.C.J. Luo, An unsymmetrical motion in a horizontal impact oscillator, *Journal of Vibration and Acoustics, Transactions of the ASME* 124 (3) (2002) 420–426.
[41] A. Kahraman, R. Singh, Non-linear dynamics of a geared rotor-bearing system with multiple clearances, *Journal of Sound and Vibration* 144 (3) (1991) 469–506.
[42] A. Kunert, F. Pfeiffer, Stochastic model for rattling in gear-boxes. Nonlinear dynamics in engineering system, in: W. Schiehlen (Ed.), *Nonlinear Dynamics in Engineering Systems*, Springer, Berlin, Heidelberg, 1990, pp. 173–180.
[43] T.J. Lin, R.F. Li, Z.G. Tao, Numerical simulation of 3-D gap type nonlinear dynamic contact-impact characteristics for gear transmission, *Chinese Journal of Mechanical Engineering* 36 (6) (2000) 55–58.
[44] H.J. Dong, Y.W. Shen, M.G. Liu, S.H. Zhang, Research on the dynamical behaviors of rattling in gear system, *Chinese Journal of Mechanical Engineering* 40 (1) (2004) 136–141.
[45] J. Guckenheimer, P.J. Holmes, *Nonlinear Oscillations, Dynamical Systems, and Bifurcations of Vector Fields*, second printing, Springer, New York, Berlin, Heidelberg, Tokyo, 1986.
[46] Y.A. Kuznetsov, *Elements of Applied Bifurcation Theory*, Springer, New York, 1998.
[47] S. Wiggins, *An Introduction to Applied Nonlinear Dynamical Systems and Chaos*, Springer, Berlin, 1990.
[48] D.K. Arrowsmith, C.M. Place, *An Introduction to Dynamical Systems*, Cambridge University Press, Cambridge, 1990.
[49] J. Carr, *Applications of Centre Manifold Theory. Applied Mathematical Sciences, Vol. 35*, Springer, Berling, Heidelberg, New York, 1981.
[50] B.D. Hassard, N.D. Kazarinoff, Y.H. Wan, *Theory and Applications of Hopf Bifurcation, London Mathematical Society Lecture Note Series*, Vol. 41, 1981.
[51] R.J. Rogers, R.J. Pick, On the dynamic spatial response of a heat exchanger tube with intermittent baffle contacts, *Nuclear Engineering and Design* 36 (1976) 81–90.
[52] B.C. Wen, F.Q. Liu, *Theory and Application of Vibratory Mechanism*, Mechanism Industry Press, Beijing, China, 1982.
[53] B.C. Wen, Y.L. Li, Q.K. Han, *Theory and Application of Nonlinear Oscillation*, Northeast University Press, Shenyang, China, 2001.